Effects of Harvest on Carbon and Nitrogen Dynamics in a Pacific Northwest Forest Catchment

Alex Abdelnour[1], Robert McKane[2], Marc Stieglitz[1,3], Feifei Pan[1,4], Yiwei Cheng[1]

[1] Department of Civil and Environmental Engineering, Georgia Institute of Technology, Atlanta, GA, USA.
[2]US Environmental Protection Agency, Corvallis, OR, USA
[3]School of Earth Atmospheric Sciences, Georgia Institute of Technology, Atlanta, GA, USA.
[4]Department of Geography, University of North Texas, Denton, TX, USA.

Abstract

We used a new eco-hydrological model, VELMA, to analyze the effects of forest harvest on catchment carbon and nitrogen dynamics. We applied the model to a 10-ha headwater catchment in the western Oregon Cascade Range where two major disturbance events have occurred during the past 500 years: a stand-replacing fire *circa* 1525 and a clearcut in 1975. Hydrological and biogeochemical data from this site and other Pacific Northwest forest ecosystems were used to calibrate the model. Model parameters were first calibrated to simulate the post-fire build-up of ecosystem carbon and nitrogen stocks in plants and soil from 1525 to 1969, the year when stream flow and chemistry measurements were begun. Thereafter, the model was used to simulate old-growth (1969-1974) and post-harvest (1975-2008) temporal changes in carbon and nitrogen dynamics. VELMA accurately captured observed changes in carbon and nitrogen dynamics before and after harvest. The interaction of hydrological and biogeochemical processes in the model provided a means for interpreting these changes. Results show that (1) losses of dissolved nutrients in the pre-harvest old-growth forest were generally low and consisted primarily of organic nitrogen and carbon; (2) following harvest, carbon and nitrogen losses from the terrestrial system to the stream and atmosphere increased as a result of reduced plant nitrogen uptake, increased soil organic matter decomposition, and high soil moisture; and (3) the rate of forest regrowth following harvest was lower than that after fire because post-clearcut stocks and turnover of detritus nitrogen were substantially lower than after fire.

1. Introduction:

Harvest and fire are two disturbances that have impacted the life history of the vegetation growth in forests of the Pacific Northwest [*Agee*, 1994; *Agee* 1990; *Franklin and Forman*, 1987; *Stednick*, 1996; *Wright and Agee*, 2004; *Wright and Heinselman*, 1973]. Forest fire and harvest in the Pacific Northwest have been found to increase water yield [*Amaranthus et al.*, 1989; *Bosch and Hewlett*, 1982; *Helvey*, 1980; *Hibbert*, 1966], summer low flow [*Keppeler and Ziemer*, 1990; *Neary et al.*, 2005], peak streamflow [*Beschta et al.*, 2000; *Harr and McCorison*, 1979; *Ice et al.*, 2004], stream nutrient concentrations [*Beschta*, 1990; *Sollins and McCorison*, 1981; *Sollins et al.*, 1981; *Tiedemann et al.*, 1988; *Raison et al.*, 1990], greenhouse gas emissions [*Harmon et al.*, 1990; *Turner et al.*, 2003], and soil microbial activity [*Bormann et al.*, 1968; *Grant et al.*, 2007]. Forest fire and harvest have also been shown to reduce evapotranspiration [*Jones and Post*, 2004; *Jones*, 2000; *Ice et al.*, 2004], plant N uptake, and forest productivity [*Sollins and McCorison*, 1981]. These changes to the ecosystem hydrological fluxes and biogeochemical dynamics affect key ecosystem services relevant to land managers and policymakers such as timber production, water quality and quantity, and wildlife habitat. For informed management decisions to be made, it is therefore important to understand how historical natural and man-made disturbances affected long-term watershed hydrology, carbon (C) and nitrogen (N) dynamics, and vegetation recovery, so as to draw insights into the impact of future managements on key ecosystem processes. Attempts at investigating the impact of forest disturbances have usually been addressed through paired-watershed experiments [*Harr and McCorison*, 1979; *Langford*, 1976; *Moore and Wondzell*, 2005; *Raison et al.*, 1990; *Weber and Flannigan*, 1997] or model simulations [*Janisch and Harmon*, 2002; *Storck et al.*, 1998; *Tague and Band*, 2000; *Wright et al.*, 2002].

A number of experimental paired watershed studies have explored the impact of harvest on ecosystem dynamics in the Pacific Northwest forests. These experimental studies have been conducted in places such as the H.J. Andrews Experimental forest in the western-central Cascade Mountains of Oregon, and the Alsea watershed study in coastal Oregon, amongst others. For example, (1) *Stednick* [2008] used long-term measurement of nutrients losses to the stream to explore the impact of forest harvest on water quality in three watersheds in coastal Oregon, and (2) *Sollins and McCorison* [1981] measured nitrogen concentration in a small experimental watershed in western Oregon, to explore the impact of clearcut on nitrogen pool and losses. Nonetheless, the complexity of experimental ecosystem studies often prevents direct interpretation of relationships between responses and specific perturbations [*Grant et al*., 2008; *Thompson et al*., 2006]. Moreover, difficulties in separating the effects of plant biomass removal from the effects of roads have been identified and known to impact experimental results [*Yanai et al.*, 2003]. Furthermore, experimental studies are usually expensive, require a significant time commitment, and cannot be used alone to quantify the contribution of specific processes to specific observed biogeochemical responses [*Alila and Beckers*, 2001; *Giesen et al*., 2008; *Stednick*, 2008].

Process-based eco-hydrological models can help address this need by providing a whole-system synthesis of disparate data sets and by exploring underlying process-level controls on catchment hydrological and biogeochemical responses to disturbance. Models can isolate the effect of a 'target' treatment factor from the effects of other factors that may be unavoidably altered within a single treatment [*McKane et al.*, 1997]. A number of models have been used to test forest management treatment scenarios, reproduce historical disturbances, and simulate post-disturbance successional changes in carbon and nitrogen, amongst others. For example: (1)

Harmon and Marks [2002] developed a carbon model STANDCARB, to examine the effects of forest management treatments such as slash burning, partial harvest and clearcut, amongst others, on plant and soil carbon pools in Pacific Northwest forests, (2) *Wimberly* [2002] used a spatial simulation model of forest succession to mimic pre-settlement landscape dynamics in the Oregon Coast Range, and (3) *Peng et al.*, [2002] used the Century model [*Parton*, 1996] to simulate the impact of different harvesting intensities and rotation lengths on the long-term carbon and nitrogen dynamics of boreal forests in central Canada. These and other simulation models have provided an effective tool to complement field research and to examine the integrated responses of watershed hydrology, ecology, and biogeochemistry to interacting stressors.

However, existing process-based models have disadvantages. Many are too simple to capture the important process-level hydrological and biogeochemical controls on ecosystem responses to disturbance. At the other extreme, some models are so complex that they require forcing data that are often unavailable, or are too computationally expensive to simulate the local dynamics over large watershed areas, or require a high level of expertise to implement. There is therefore need for a balanced approach. Specifically an accessible, spatially-distributed, ecohydrological model that is both computationally efficient and relatively easy to implement for analyzing the potential effects of changes in climate, land-use and land cover on watershed hydrological and biogeochemical processes.

We use such an ecohydrological model, VELMA (Visualizing Ecosystems for Land Management Assessments, [*Abdelnour et al*., 2011]), to investigate the response of Pacific Northwest forests to harvest. Specifically, we apply the model to a small intensively studied catchment (WS10), where a stand-replacing fire occurred in 1525 and a 100% clearcut in 1975. First, we calibrate the model to simulate the build-up of ecosystem C and N stocks from the

onset of the stand replacing fire of 1525 to 1969 the first year with available streamflow and C and N data. Thereafter, we explore the temporal changes in measured and unmeasured biogeochemical fluxes such as nutrient losses, soil heterotrophic respiration, and N_2-N_2O emissions, amongst others, for two periods of interest: (1) during old-growth condition when the ecosystem was relatively close to steady state (1969 to 1974), and (2) following the 1975 whole catchment clearcut (1975 to 2008). Section 2 of this paper describes the study site. Section 3 provides an overview of the VELMA modeling framework. Section 4 describes the simulation methods, the calibration and the sensitivity analysis. Section 5 presents model results and discussion. Section 6 summarizes our major conclusions.

2. Site Description

Watershed 10 (WS10) of the H.J. Andrews Experimental Forest (HJA) is a small 10.2 hectare catchment located in the western-central Cascade Mountains of Oregon, at latitude 44°15′N, longitude 122°20′W (Figure 1). Watershed 10 has been the site of intensive research and manipulation by the U.S. forest Service since the 1960's, mainly to study the effects of forest harvest on hydrology, sediment transport, and nutrient loss [*Dyrness*, 1973; *Fredriksen*, 1975; *Harr and McCorison*, 1979; *Jones and Grant*, 1996; *Rothacher*, 1965; *Sollins and McCorison*, 1981; *Sollins et al.*, 1981].

Watershed 10 elevation ranges from 430 m at the stream gauging station to 700 m at the southeastern ridgeline. Near-stream and side-slope gradients are approximately 24° and 25° to 50°, respectively [*Grier and Logan*, 1977; *Sollins et al.*, 1981]. The climate is relatively mild with wet winters and dry summers [*Grier and Logan*, 1977]. Mean annual temperature is 8.5°C. Daily temperature extremes vary from 39°C in the summer to -20°C in the winter [*Sollins and McCorison*, 1981]. Mean annual precipitation is 2,300 mm and falls primarily as rain between

October and April [*Jones and Grant*, 1996]. Snow rarely persists longer than a couple of weeks and usually melts within 1 to 2 days [*Harr and McCorison*, 1979; *Harr et al.*, 1982; *Jones*, 2000]. Soils are of the Frissel series, which are classified as Typic Dystrochrepts with fine loamy to loamy-skeletal texture [*Sollins et al.*, 1981; *Vanderbilt et al.*, 2003] and are generally deep and well drained [*Grier and Logan*, 1977].

Two significant events determined the life history of the vegetation growth in WS10; a stand-replacing fire event in 1525 [*Wright et al*., 2002] and a man-made clearcut in 1975 [*Sollins and McCorison*, 1981]. Prior to the 100% clearcut in 1975, WS10 was a 450 year-old forest dominated by Douglas-fir (*Pseudotsuga menziessii*), western hemlock (*Tsuga heterophylla*), and western red cedar (*Thuja plicata*) [*Grier and Logan*, 1977] reaching up to ~60 m in height, with rooting depths rarely exceeding 100 cm [*Santantonio et al.*, 1977]. In the spring of 1975, WS10 was clearcut. All trees and woody materials larger than 20 cm in diameter or 2.4 m in length, including many logs on the ground, were removed from the site. Large woody slash was disposed of without burning [*Gholz et al.,* 1985]. Post-clearcut residual plants consisted of understory shade tolerant vegetation and shrubbery, undamaged by harvest [*Gholz et al.,* 1985]. Species such as the vine maple (*Acer circinatum*), Pacific rhododendron (*Rhododendron maximum*) and chinkapin (*Castanopsis chrysophylla*) regenerated during the spring after logging. In 1976, one year after clearcut, WS10 was planted with 2-year-old seedlings of Douglas-fir [*Gholz et al.,* 1985]. The dominant vegetation of WS10 today is a ~35 year-old mixed Douglas-fir and western hemlock stand.

3. The Eco-Hydrological Model

We have developed a spatially distributed ecohydrological model, VELMA, to simulate changes in soil water infiltration and redistribution, evapotranspiration, surface and subsurface

runoff, carbon and nitrogen cycling in plants and soils, and the transport of dissolved forms of carbon and nitrogen from the terrestrial landscape to streams. VELMA is designed to simulate the integrated responses of ecohydrological processes to multiple forcing variables, e.g., changes in climate, land-use and land cover. It is intended to be broadly applicable to a variety of ecosystems (forest, grassland, agricultural, tundra, etc.) and to provide a computationally efficient means for scaling up ecohydrological responses across multiple spatial and temporal scales – hillslopes to basins, and days to centuries. A detailed description of the biogeochemical component of VELMA is provided in Appendix A. [Note: The hydrological component of VELMA was presented in *Abdelnour et al.,* [2011] and will not be described in the current manuscript]

The model uses a distributed soil column framework to simulate the movement of water and nutrients (organically bound carbon (C) and nitrogen (N) in plants and soils; dissolved inorganic nitrogen (DIN), dissolved organic nitrogen (DON) and dissolved organic carbon (DOC); and gaseous forms of C and N including CO_2, N_2O and N_2) within the soil, between the soil and the vegetation, and from the soil surface and vegetation to the atmosphere. The soil column model consists of three coupled sub-models: (1) a *hydrological model* (Figure A.2, Appendix A) that simulates vertical and lateral movement of water within soil, losses of water from soil and vegetation to the atmosphere, and the growth and ablation of the seasonal snowpack – the hydrological model is described in Appendix A of *Abdelnour et al.,* [2011], (2) a *soil temperature model* [*Cheng et al.*, 2010] that simulates daily soil layer temperatures from surface air temperature and snow depth by propagating the air temperature first through the snowpack and then through the ground using the analytical solution of the one-dimensional thermal diffusion equation (Equations 1-6, Appendix A), and (3) a *plant-soil model* (Figure A.3,

Appendix A) that simulates ecosystem carbon storage and the cycling of C and N between a plant biomass layer and the active soil pools. Specifically, the plant-soil model simulates the interaction between aboveground plant biomass, soil organic carbon (SOC), soil nitrogen including dissolved nitrate (NO_3), ammonium (NH_4), and organic nitrogen, as well as dissolved organic carbon (Equations 7-12, Appendix A). Daily atmospheric inputs of wet and dry nitrogen deposition are accounted for in the ammonium pool of the shallow soil layer (Equation 13, Appendix A). Uptake of ammonium and nitrate by plants is modeled using a Type II Michaelis-Menton function (Equation 14, Appendix A). Loss of plant biomass is simulated through a density dependent mortality. The mortality rate and the nitrogen uptake rate mimic the exponential increase in biomass mortality and the accelerated growth rate, respectively, as plants go through succession and reach equilibrium (Equations 14-18, Appendix A). Vertical transport of nutrients from one layer to another in a soil column is function of water drainage (Equations 19-22, Appendix A). Decomposition of soil organic carbon follows first order kinetics controlled by soil temperature and moisture content as described in the TEM model (Terrestrial Ecosystem Model) of *Raich et al.,* [1991] (Equations 23-26, Appendix A). Nitrification (Equations 27-30, Appendix A) and denitrification (Equations 31-34, Appendix A) were simulated using the equations from the generalized model of N_2 and N_2O production of *Parton et al.,* [1996; 2001] and *Del Grosso et al.,* [2000].

The soil column model is placed within a catchment framework to create a spatially distributed model applicable to watersheds and landscapes. Adjacent soil columns interact with each other through the downslope lateral transport of water and nutrients (Figure A.1, Appendix A). Surface and subsurface lateral flow are routed using a multiple flow direction method [*Freeman*, 1991; *Quinn et al.*, 1991]. As with vertical drainage of soil water, lateral subsurface

downslope flow is modeled using a simple logistic function and corrected for the local topographic slope angle. Lateral transport of nutrients from one soil column to the subsequent soil column or towards the stream is simulated as a function of subsurface flow and nutrient-specific loss rates (Equations 35-38, Appendix A). Nutrients transported downslope from one soil column to another can be processed through the different C and N cycling sub-models in that downslope soil column, or continue to flow downslope, interacting with other soil columns, or ultimately discharging water and nutrients to the stream.

4. Simulation Methods

4.1. Data

The model is forced with daily temperature, precipitation, and atmospheric nitrogen deposition. Observed daily temperature and precipitation data for the period January 1, 1969 - December 31, 2008 were obtained from the H.J. Andrews LTER PRIMET, CS2MET, and H15MET meteorological stations located around WS10 [*Daly and McKee*, 2011] (see Figure 1). At the H.J. Andrews Experimental forest, observed wet atmospheric nitrogen deposition is available approximately every 3 weeks, for the period 1968 to 2010, whereas observed dry atmospheric nitrogen deposition is available 2 to 4 times a year, for the period 1988 to 2010 [*Johnson and Fredriksen*, 2010]. However, for the purpose of our simulations, we will use the average annual value of the total wet and dry nitrogen deposition found by *Sollins et al.*, [1980] (Equation 13 in Appendix A). *Sollins et al.*, [1980] measured the average wet and dry nitrogen deposition in WS10 for the period 1973 to 1975 and found that annual N input in precipitation and dust were ~0.2 $gNm^{-2}yr^{-1}$. This average annual value is then partitioned based on the ratio of daily precipitation to the average (1969-2008) annual precipitation.

Observed data used for model calibration and validation include daily streamflow measured at the WS10 weir between 1969 to 2008 [*Johnson and Rothacher*, 2009], and NO_3, NH_4, DON and DOC losses to the stream measured for flow-weighted, composite samples collected approximately once every three weeks for the period 1978 to 2007, except DOC for which the period of record is 1992 to 2007 [*Johnson and Fredriksen*, 2011]. A 30-m resolution Digital Elevation Model of the H.J. Andrews's WS10 [*Valentine and Lienkaemper*, 2005] was used to compute flow direction, delineate watershed boundaries, and generate a channel network. Each 30x30-meter soil column was divided into 4 layers and was assumed to have an average soil column depth to bedrock of 2 m [*Ranken*, 1974]. The dominant soil texture was specified as loam [*Ranken*, 1974]. Porosity, field capacity and wilting point values were obtained following *Dingman*, [1994].

4.2. Model Calibration and C and N "spin-up"

4.2.1. Hydrological parameters calibration

Abdelnour et al., [2011] previously calibrated and validated VELMA's hydrological parameters to simulate pre- and post clearcut temporal changes in WS10's streamflow. Specifically, model hydrological parameters such as the surface hydraulic conductivity, soil layer thicknesses, ET shape factor and snowmelt parameters were calibrated to (1) reproduce the observed daily streamflow for the period 1969 to 2008, (2) capture the observed subsurface dynamics in WS10 (i.e., preferential lateral transport of water at the soil-bedrock interface [*Ranken*, 1974; *Van Verseveld et al.*, 2008]), and (3) mimic the rapid runoff response to rainfall [*Kirchner*, 2003; *Ranken*, 1974]. Hydrological parameter names, values and references can be found in Table A.1 and Table A.2 in Appendix A of *Abdelnour et al.*, [2011].

4.2.2. Biogeochemical parameters calibration

A post-fire "build-up" simulation was conducted for the period 1525-1968 (Figure 2) in order to identify, through calibration, a single set of parameters that captures the accumulation of ecosystem C and N stocks following a stand-replacing fire in 1525 [*Grier and Logan*, 1977; *Wright et al*., 2002] to 1968. Daily temperature and precipitation drivers were constructed from a continuous loop of the available 1969 to 2008 observed climate station data. Typically following stand-replacing fires a large fraction of plant biomass is converted from live to dead matter [*Janisch and Harmon*, 2002], and a much smaller fraction is combusted as CO_2 [*Mitchell et al.*, 2009]. Consequently, there is a correspondingly large increase in coarse detrital matter that decomposes slowly during the decades following fire [*Janisch and Harmon*, 2002]. Therefore, the post-fire simulation was initialized by (1) reducing the initial live plant biomass value to 1% of its pre-fire old-growth value [*Wright et al*., 2002], (2) converting the dead plant biomass into detrital (soil) organic carbon [*Wright et al*., 2002], and (3) reducing the transpiration rate to zero initially, followed by an asymptotic increase to pre-disturbance values within 50 years [*Abdelnour et al*., 2011]. The 1525 initial conditions of plant biomass and soil organic carbon are 450 gCm^{-2} and 70,000 gCm^{-2}, respectively. Model parameters such as plant uptake rate, plant mortality rate, and soil organic carbon decomposition rate were calibrated to achieve a biomass buildup trajectory (1525-1968) that passed through observed chronosequence data taken at WS10 and other Pacific Northwest (PNW) forest ecosystems [*Grier and Logan*, 1977; *Harmon et al.*, 2004; *Janisch and Harmon*, 2002; *Smithwick et al.*, 2002; *Sollins and McCorison*, 1981; *Sollins et al.*, 1980] (Figure 3 and Table 1). Calibration parameters determined from this post-fire "build-up" simulation were then considered fixed for all subsequent WS10 simulations. A detailed description of the catchment biogeochemical

dynamics associated with this calibration simulation is provided in section 5.1. Biogeochemical parameter names, values and references are provided in Tables B.1.

4.3. Sensitivity Analysis

We employ the method described by *Mckane et al* [1997] to conduct a sensitivity analysis of the model's calibrated parameters. This sensitivity analysis includes two parts. Part 1 examines the model's sensitivity to VELMA's most important hydrological and biogeochemical parameters. Specifically we choose 3 hydrological parameters – surface hydraulic conductivity, lateral and vertical decay of the hydraulic conductivity with depth – and 6 biogeochemical parameters – Loss rates for nitrate, ammonium, DON and DOC, carbon decomposition rate into the DON pool, and average annual nitrogen deposition. Based on our experience with calibrating the model, these parameters were clearly the most important in affecting hydrological and biogeochemical outputs. We examined the model's sensitivity to each of these parameters individually by increasing or decreasing the calibrated value by 10% and 20%, then re-running the model for all of the experimental treatments. We calculated the absolute differences between simulated and measured data for each of the five output variables (streamflow, NO_3, NH_4, DON, and DOC losses) for which high quality observed data are available – in particular, observed stream flow and chemistry for WS10's pre-harvest (1969-1974) and post-harvest (1975-2008) periods of record, and normalized it against the absolute differences between the original simulated results and the observed data. For each adjustment in variable, an error term was calculated to assess parameter sensitivity, and used to help identify whether a given set of parameter values represents a best fit of the model to the observed data [*McKane et al,* 1997]:

$$E = \left(\sum_{i=1}^{5} \frac{(S_i - O_i)}{(S_{i,o} - O_i)}\right) / 5$$

where E is the normalized absolute error, S_i is the simulated output (e.g streamflow), O_i is corresponding observed output, and $S_{i,o}$ is the original simulated output. If E=1, the adjustment in variable did not result in any change in the absolute error. For E>1, the adjustment in variable increased the absolute error, and for E<1, the adjustment in variable decreased the absolute error.

Part 2 of our sensitivity analysis examined how the overall error term changes when VELMA is calibrated to favor alternative flow pathways. The model is currently optimized for deep flow paths [*Abdelnour et al.*, 2011] – those favoring rapid vertical flow and subsequent lateral flow along the soil-bedrock interface to the stream – that *Ranken* [1974], *Van Verseveldet al.*, [2008], and *Kirchner*, [2003] identified through their experimental studies as the predominant flow path in WS10. Alternatively, by changing soil layer thickness to have (1) equal soil layer thickness along the soil profile, which favors deep flow and slow runoff response to rainfall, or (2) a geometric progression of soil layer thickness along the soil profile, which favors shallow subsurface runoff and deep storage of water, we evaluated how well such a parameterization compares to the current one that is more consistent with available experimental data. Results of the sensitivity analysis showed that, for both Parts 1 and 2 of the sensitivity analysis, all of the E calculated are > 1 (Table 2 and Figure 4), indicating that the current model calibration provides the best fit to the measured data.

4.4. Pre- and Post Clearcut Simulations

1) *A pre-clearcut "old growth" simulation* was conducted for the period 1969-1974 (Figure 2) to explore daily, seasonal, and annual changes in C and N dynamics when the ecosystem was close to steady state conditions [*Sollins et al.*, 1980]. Initial values of plant biomass, SOC, NH_4, NO_3, DON and DOC pool were determined from the 1525-1968 post-fire

"build-up" simulation. A detailed description of the simulated nutrient flux dynamics for the old-growth period is provided in section 5.2.

2) *A post-clearcut simulation* was conducted for the period 1975-2008 (Figure 2) in order to explore the impact of clearcut on measured and unmeasured nutrient losses, soil heterotrophic respiration, and N_2-N_2O land-atmosphere emissions, amongst others. Watershed 10 was a 100% clearcut in the spring of 1975. All trees and woody material larger than 20 cm in diameter or 2.4 m in length were removed from the site [*Sollins and McCorison*, 1981; *Halpern and Spies*, 1995]. The residual plants after the 1975 clearcut consisted of understory shade tolerant plants and shrubbery, undamaged by harvest [*Grier and Logan*, 1977; *Gholz et al.*, 1985]. To mimic the 1975 spring clearcut, the initial live plant biomass value was reduced to 10% (~ 4,500 gCm^{-2}) of its pre-harvest value [*Gholz et al.*, 1985; *Lee et al*., 2002] and the soil organic carbon pool was increased by 10% to account for new inputs of dead roots and stumps (all other plant biomass was assumed to have been removed from the site as logs) [*Grier and Logan*, 1977; *Gholz et al.*, 1985]. Plant transpiration rates were set to zero in 1975 and then increased asymptotically to pre-disturbance values within 50 years [*Abdelnour et al*., 2011]. A detailed description of the simulated nutrient fluxes dynamics for the post-harvest period is provided in section 5.3.

5. Simulation Results and Discussion

Results and discussion are generally presented in the following sequence: (1) changes in plant biomass and SOC, (2) changes in dissolved organic and inorganic C and N losses to the stream, (3) changes in gaseous losses of C and N to the atmosphere, and (4) changes in net primary production (NPP) and net ecosystem production (NEP).

5.1. Post-fire "build-up" of Ecosystem C and N Stocks (1525-1968)

5.1.1. Post-Fire Plant Biomass and SOC (1525-1968)

Post-fire simulated plant biomass increased from the 1525 value of 450 gCm^{-2} at an average rate of 580 $gCm^{-2}yr^{-1}$ for the first 30 years and at a rate of 300 $gCm^{-2}yr^{-1}$ for the next 70 years (Figure 3). Thereafter, simulated plant biomass gradually leveled off, reaching an old-growth value of ~42,500 gCm^{-2} after approximately 400 years. Post-fire SOC decreased exponentially from the 1525 value of ~70,000 gCm^{-2} as a result of high decomposition and low detritus input to the soil, and reached its lowest level after about 100 years (Figure 3). At that point, re-growing plant biomass provided increasing amounts of detritus input to the soil, thereby replenishing the soil carbon pool. Soil carbon subsequently rose and stabilized at ~25,600 gCm^{-2}, 300 years into the simulation (Figure 3). Simulated post-fire recovery of plant biomass and SOC were generally consistent with observed successional changes in live and dead wood carbon stores in other forests of the PNW [*Janisch and Harmon*, 2002; *Spies et al.*, 1988; *Turner et al.*, 2004]. However, early (less than 100 years old) simulated successional rates of increase in plant biomass exceeded the reported observed values by *Janisch and Harmon*, [2002] (see Figure 3). In Figure 3, observed data for all stands less than 100 years old were after clearcut, whereas all stands older than 100 years were after a stand replacing fire. As a result, the difference between observed and simulated early successional plant biomass may owe in part to the greater amount of nitrogen released from decomposing detritus following fire than after clearcut.

5.1.2. Post-Fire Gaseous C and N losses (1525-1968)

Post-fire simulated gaseous losses of C and N increased as a result of high SOC decomposition, high soil water content, and low levels of plant N uptake. Specifically, simulated soil heterotrophic respiration (R_h) followed a similar trajectory as SOC, peaking (1,500 $gCm^{-2}yr^{-1}$) in the year 1525, and then falling exponentially until reaching its lowest value 120 years after disturbance (Figure 5). Thereafter, R_h increased with increasing SOC and reached an

equilibrium value of ~488 $gCm^{-2}yr^{-1}$. Post-fire simulated soil denitrification rates (N_2 and N_2O emissions to the atmosphere) increased rapidly and peaked 8 years after disturbance. Thereafter, soil denitrification decreased exponentially due to a reduction in soil nitrate availability and reached a steady state value of ~0.06 $gNm^{-2}yr^{-1}$ approximately 300 years into the simulation. Similar results were found by *Turner et al.,* [2003] who used the carbon cycle model, Biome-BGC, to explore the temporal dynamics of carbon fluxes in two western Oregon watersheds. *Turner et al.,* [2003] found that R_h peaked (~1,300 $gCm^{-2}yr^{-1}$) at the onset of the disturbance, then decreased exponentially and reached equilibrium value (~600 $gCm^{-2}yr^{-1}$) within 200 years.

5.1.3. Post-Fire NPP and NEP (1525-1968)

As a result of vegetation removal and the large soil decomposition-driven losses of C as CO_2 to the atmosphere and as DOC to the stream, the initial 1525 post-fire simulated value of NPP and NEP was 90 $gCm^{-2}yr^{-1}$ and -1,500 $gCm^{-2}yr^{-1}$, respectively (Figure 5). Thereafter, simulated NPP increased with increasing N availability in the soil, reached a peak value of ~1,300 $gCm^{-2}yr^{-1}$ 14 years after fire, then decreased exponentially due to the decrease in N availability, and finally reached a stable value of ~500 $gCm^{-2}yr^{-1}$ within 200 years. Similarly, post-fire simulated NEP increased with the rapid regrowth of plant biomass and became positive, peaking at ~150 $gCm^{-2}yr^{-1}$ after only 15 years. Thereafter, NEP decreased exponentially, reaching a steady state average equilibrium value of ~9 gCm^{-2} after 200 years. Post-fire changes in NPP and NEP are generally consistent with a variety of chronosequence observations and modeling studies (Figure 6) [e.g. *Luyssaert et al.,* 2008*; Turner et al.,* 2003; *Hicke et al.,*2003*; Law et al.,* 2001, and *Janisch and Harmon*, 2002, amongst others]. For example, *Turner et al.,* [2003] used the Biome-BGC model to analyze forest carbon dynamics in the H.J. Andrews forest and found that (1) NPP was near zero early in succession, increased and reached 1,200 $gCm^{-2}yr^{-}$

[1], 15 years after disturbance, then decreased exponentially and reached an equilibrium value of ~620 $gCm^{-2}yr^{-1}$ within 200 years, and (2) NEP was strongly negative (~ -1,300 $gCm^{-2}yr^{-1}$) at the onset of the disturbance, peaked at ~700 $gCm^{-2}yr^{-1}$ 15 years after disturbance, then decreased exponentially and reached an equilibrium value of ~20 $gCm^{-2}yr^{-1}$ within 200 years.

5.2. Old-Growth Biogeochemical Dynamics (1969-1974)

At daily time scales, simulated nutrient losses were generally high in the wet season and low in the summer dry season. Specifically, simulated daily NH_4 losses averaged 0.06 $mgNm^{-2}day^{-1}$ and were strongly correlated to precipitation (R^2=0.8) and stream discharge (R^2=0.6). NH_4 losses peaked in fall and winter with the peaks in streamflow and reached 1.2 $mgNm^{-2}day^{-1}$. Summer NH_4 losses were low, averaging 0.03 $mgNm^{-2}day^{-1}$. Simulated daily NO_3 losses averaged 0.02 $mgNm^{-2}day^{-1}$ and were strongly correlated to streamflow (R^2=0.7), but weakly correlated to precipitation (R^2=0.4). Simulated NO_3 losses were largest (1) in the summer as a result of high nitrification rates, and (2) in the fall, at the onset of the rainy season when hydrological connectivity within hillslopes is re-established and nutrients accumulated in soils during drier summer months are more readily flushed downslope [*Creed et al.*, 1996; *Stieglitz et al.*, 2003]. Simulated daily DOC and DON losses averaged 7.6 $mgCm^{-2}day^{-1}$, and 0.5 $mgNm^{-2}day^{-1}$, respectively, and were strongly correlated to stream discharge (R^2=0.8 and 0.9, respectively). Dissolved organic carbon and dissolved organic nitrogen losses peaked with peakflow, reaching 115.5 $mgCm^{-2}day^{-1}$ and 6.7 $mgNm^{-2}day^{-1}$, respectively, and were largest in fall and winter. In the summer season, DOC and DON losses were minimal and averaged 0.8 $mgCm^{-2}day^{-1}$ and 0.05 $mgNm^{-2}day^{-1}$, respectively. Similar results have been found by *Vanderbilt et al.*, [2003], who analyzed long-term organic and inorganic nitrogen outputs in stream water in six watersheds at the H.J. Andrews Experimental Forest in Oregon. They found

that NH_4, NO_3 and DON losses to the stream were correlated to stream discharge with a R^2 of 0.5, 0.5, and 0.8, respectively. Note: observed daily nutrient losses data for the period 1969 to 1975 were unavailable at WS10 for a comparison with our simulated daily values.

On an annual basis, simulated losses of dissolved inorganic nitrogen (NH_4 and NO_3) averaged 0.03 $gNm^{-2}yr^{-1}$ with NH_4 losses being three times NO_3 losses to the stream (NO_3/NH_4 ~33%). Specifically, simulated annual NO_3 and NH_4 losses averaged 0.008 $gNm^{-2}yr^{-1}$ and 0.023 $gNm^{-2}yr^{-1}$, respectively. Simulated annual DON losses averaged 0.14 $gNm^{-2}yr^{-1}$ and accounted for 81% of the nitrogen that reached the stream (DON/DIN = 4.4). Simulated annual DOC losses averaged 2.9 $gCm^{-2}yr^{-1}$ and ranged between 1.7 and 4.5 $gCm^{-2}yr^{-1}$. These simulated old-growth nutrient fluxes were consistent with other studies of the biogeochemical dynamics of old-growth forests in the PNW (Table 3). For example, *Sollins and McCorison* [1981] measured nitrogen and carbon solution chemistry in WS10 before the 1975 clearcut, and found that, in an undisturbed watershed, NH_4 accounted for 18 to 33% of total dissolved nitrogen, DON accounted for the rest, and NO_3 concentration was very low. Similarly, *Fredriksen* [1975] found that nitrogen losses in undisturbed forests are small and occur primarily as DON.

5.3. Post-Harvest Biogeochemical Dynamics (1975-2008)

To explore the impact of the 1975 WS10 clearcut on C and N dynamics, we conducted two simulations: a post-harvest simulation for the period 1975 to 2008 (described in section 4.2), and a control simulation, over the same period, in which no vegetation is removed (i.e. soil and plant C and N dynamics are at steady state and similar to old-growth dynamics, Table 1 and 3). Post-clearcut simulated relative changes in C and N fluxes are presented in terms of the difference between the post-harvest simulation values and the control simulation values.

5.3.1. Post-Clearcut Plant biomass and SOC (1975-2008)

Simulated post-clearcut plant biomass increased rapidly at a rate of ~400 $gCm^{-2}yr^{-1}$ as a result of large early successional N uptake rates and N availability, and reached a value of ~ 16,000 gCm^{-2}, thirty years after disturbance. Simulated post-clearcut SOC decreased as a result of high SOC decomposition and low detritus input into the soil. Simulated SOC reached 55% of its initial value (~15,000 gCm^{-2}) thirty years after clearcut. Simulated recoveries of plant biomass and SOC were consistent with observed early successional changes in live and dead wood carbon stores in PNW forests [*Janisch and Harmon*, 2002; *Spies et al.*, 1988]. However, post-clearcut simulated successional rates of change in plant biomass and SOC exceeded the reported observed values by *Janisch and Harmon*, [2002]. *Janisch and Harmon*, [2002] found that live tree bole carbon stores increased after disturbance and reached ~7,500 gCm^{-2} (i.e. ~9,500 gCm^{-2} for total plant biomass), thirty years after disturbance. Moreover, *Janisch and Harmon*, [2002] found that coarse woody detritus carbon stores decreased after clearcut and reached 50% of its initial mass (~2,800 gCm^{-2}), thirty years after disturbance. Nevertheless, *Janisch and Harmon*, [2002] simulated old-growth values of live and dead carbon stores (31,900 gCm^{-2} and 7,200 gCm^{-2}, respectively) were generally at the lower end of the range reported for Oregon forests (29,500-58,500 gCm^{-2} [*Grier and Logan*, 1977; *Harmon et al.*, 2004] and 12,700-32,600 gCm^{-2} [*Grier and Logan*, 1977; *Harmon et al.*, 2004; *Means et al.*, 1992]).

5.3.2. Post-Clearcut Dissolved C and N losses (1975-2008)

Post-clearcut losses of dissolved inorganic N to the stream peaked a few years after disturbance as a result of high SOC decomposition, low levels of plant N uptake prior to significant re-establishment of plant biomass, and the increase in streamflow. Specifically, simulated annual NH_4 and NO_3 losses peaked 2 years after clearcut, and averaged 0.08 $gNm^{-2}yr^{-1}$ (4-fold higher than control values) and 0.9 $gNm^{-2}yr^{-1}$ (150-fold higher than control values),

respectively, over the first five years. Thereafter, simulated annual NH_4 and NO_3 losses decreased as a result of a decreasing SOC pool and an increase in N uptake by plants, and reached 0.015 $gNm^{-2}yr^{-1}$ (25% lower than control values) and 0.008 $gNm^{-2}yr^{-1}$ (10% lower than control values), respectively, thirty years after clearcut. The simulated changes in NH_4 and NO_3 losses to the stream were consistent with observed data at WS10 (see Figure 8 and Table 4) as well as previously published studies of biogeochemical dynamics in recently clearcut old-growth forests [e.g. *Cairns and Latjtha* 2005; *Sollins and McCorison*, 1981; *Fredriksen* 1975]. For example, *Sollins and McCorison* [1981] found that NO_3 concentration increased as much as 100-fold, 7 to 18 months after the 1975 clearcut of WS10. *Fredriksen* [1975] found that following forest clearcut at two experimental watersheds in western Oregon, sharp increases in stream N concentrations were attributed to decreased plant N uptake and increased detritus N subject to mineralization into ammonium. *Vitousek and Reiners* [1975] found that vegetation removal by fire or forest harvest results in an immediate but transient flush of N to streams, which is quickly followed by tight retention of N in young vigorously growing stands.

Post-clearcut simulated dissolved organic C and N losses to the stream were driven by high SOC decomposition and high subsurface flow. Specifically, simulated annual DON and DOC losses peaked two years after clearcut, and averaged 0.15 $gNm^{-2}yr^{-1}$ (~20% higher than control values) and 3.2 $gCm^{-2}yr^{-1}$ (~18% higher than control values) over the first five years, respectively. Thereafter, simulated annual DON and DOC losses decreased with decreasing SOC and averaged 0.07 $gNm^{-2}yr^{-1}$ (~30% lower than control values) and 1.1 $gCm^{-2}yr^{-1}$ (~35% lower than control values) thirty years after clearcut, respectively. Changes in DON and DOC losses to the stream were consistent with observed post-clearcut nutrients dynamics in WS10 (see Figure 8 and Table 4) and other PNW forests. *Cairns and Latjtha* [2005] found that DON

and DOC losses in young watersheds were approximately 30% and 25% higher than in old watersheds. *Sollins and McCorison* [1981] found that DOC concentrations were higher in the clearcut watershed compared to the control watershed.

5.3.3. Post-Clearcut Gaseous C and N losses (1975-2008)

Post-clearcut simulated gaseous losses of C and N increased as a result of high SOC decomposition, high soil water content, and low levels of plant N uptake prior to significant plant regrowth. Specifically, simulated annual denitrification rates and soil heterotrophic respiration (R_h) peaked two years after clearcut, and averaged 0.9 $gNm^{-2}yr^{-1}$ (~13-fold higher than control values) and ~710 $gCm^{-2}yr^{-1}$ (30% higher than control values) from 1975 to 1980, respectively (Figure 7). Thereafter, simulated annual denitrification rates and R_h decreased with increasing plant biomass, increasing N uptake, and decreasing SOC and soil water content. By 2005, thirty years after clearcut simulated annual denitrification rates and R_h averaged 0.07 $gNm^{-2}yr^{-1}$ (30% lower than control values) and 280 $gCm^{-2}yr^{-1}$ (40% lower than control values), respectively. The simulated changes in gaseous losses of C and N were consistent with previously published studies of biogeochemical dynamics in recently clearcut old-growth forests. For example, *Grant et al.,* [2007] used an ecosystem model *ecosys* [*Grant et al.,* 2001] to simulate the impact of clearcutting on R_h in an old-growth forest of the PNW, and found that R_h peaked (~1,200 $gCm^{-2}yr^{-1}$) two years after clearcut and then decreased and reached ~350 $gCm^{-2}yr^{-1}$, 50 years after clearcut. *Griffiths and Swanson* [2001] measured the microbiological characteristics of forest soils in recently harvested and old-growth Douglas-fir in the HJA Forest, and found that the denitrification rate increased six-fold five years after clearcut, then decreased and was 20% lower than old-growth values, for a 40-year-old stand.

5.3.4. Post-Clearcut NPP and NEP (1975-2008)

Post-clearcut simulated NPP and NEP decreased from an old-growth value of 498 $gCm^{-2}yr^{-1}$ and 9 $gCm^{-2}yr^{-1}$ respectively, as a result of vegetation removal, and large decomposition-driven losses of C as CO_2 to the atmosphere and as DOC to the stream (Figure 8). Specifically, simulated annual NPP decreased by 45%, to ~390 $gCm^{-2}yr^{-1}$ at the onset of clearcut, then increased with the rapid re-growth of plant biomass, and peaked (~700 $gCm^{-2}yr^{-1}$) seven years after clearcut. Thereafter, annual NPP decreased and reached an average value of ~300 $gCm^{-2}yr^{-1}$ (~ 45% lower than control values), thirty years after clearcut. Similarly, simulated annual NEP dropped to -250 $gCm^{-2}yr^{-1}$ at the onset of the clearcut, peaked at 75 $gCm^{-2}yr^{-1}$ seven years after disturbance as a result of rapid regrowth of plant biomass, high N uptakes, and a decrease in soil C losses, and then decreased and reached 12 $gCm^{-2}yr^{-1}$, thirty years after clearcut. The simulated early successional trends in NPP and NEP are generally consistent with a variety of chronosequence simulations of recently clearcut forests of the PNW [e.g. *Grant et al.,* 2007; *Turner et al.,* 2004; *Janisch and Harmon*, 2002]. *Grant et al.,* [2007] simulated the change in NEP with forest age in a coastal Douglas–fir forest of the PNW, and found that NEP decreased (-620 $gCm^{-2}yr^{-1}$) at the onset of the disturbance, then became positive, and peaked (~450 $gCm^{-2}yr^{-1}$) ~ 18 years after clearcut. *Janisch and Harmon*, [2002] found that post-clearcut NEP was negative (-250 $gCm^{-2}yr^{-1}$) at the onset of clearcut, increased and became positive 12 to 14 years after disturbance, then peaked at ~200 $gCm^{-2}yr^{-1}$, 50 to 70 years after disturbance. However, post-clearcut NEP values simulated by VELMA for WS10 were less than simulated NEP values of other PNW forest, and were negative for a shorter period of time. This difference might be due in part to (1) the simulated removal of slash and woody debris from the clearcut watershed, which has been found to hastened the recovery of simulated NEP [*Grant et al.,* 2007] and (2)

VELMA's simplified assumption of a single stand instead of complex regenerating stands, which has been found to introduce a bias towards lower NEP [*Grant et al.,* 2007].

6. Conclusion

The ecohydrological model presented here, VELMA, provides a relatively simple, spatially distributed framework for assessing the effects of changes in climate, land-use (harvest, fire, etc.) and land cover on hydrological, ecological, and biogeochemical processes within watersheds. VELMA was used as a heuristic tool to provide process-level insights into the impact of forest fire and harvest on catchment biogeochemical fluxes at a small intensively studied catchment in the Pacific Northwest (WS10) – details that would be difficult or impossible to capture through experimentation or observation alone. Moreover, VELMA provides a framework for understanding how limited supplies of available N tightly constrains ecosystem responses (production and accumulation of biomass, net ecosystem production, etc.) to major disturbances in WS10, and perhaps, more generally for Douglas-fir dominated forests in the western Oregon Cascades of the Pacific Northwest. Although the impact of disturbances on catchment biogeochemical fluxes have already been investigated in earlier experimental studies [e.g., *Sollins and McCorison,* 1981; *Sollins et al*., 1980, *Vitousek and Reiners,* 1975; *Vitousek et al*., 1979; amongst others), the interaction of hydrological and biogeochemical processes represented in VELMA provide additional insight into how feedbacks among the cycles of C, N and water regulate N supplies. The main insights from this exercise include the following:

1) Following harvest, nutrient losses from the terrestrial system to the stream were tightly constrained by the hydrological cycle, particularly at the hillslope scale. Losses of NH_4, DON, and DOC to the stream were primarily driven by wet-season rain events that were large enough to generate hydrologic connectivity and flushing of nutrients down hillslopes. By contrast,

losses of nitrate to the stream were less predictable, owing to complex spatial and temporal patterns of nitrification and denitrification (e.g., hillsope vs. riparian zone).

2) Gaseous losses of C and N to the atmosphere, following disturbance, were primarily driven by high soil water content, high soil organic carbon decomposition, and low N uptake. Specifically, post-disturbance increase in soil moisture and nitrate availability enhanced the anaerobic process of soil denitrification and increased N_2-N_2O emissions to the atmosphere, whereas post-disturbance increase in soil organic carbon decomposition enhanced soil heterotrophic respiration and increased CO_2 emission to the atmosphere.

Although this exercise is intended to illustrate how a process-based ecohydrological modeling framework can provide useful insights into ecosystem responses to disturbance, we emphasize that VELMA uses a simplified modeling approach with comparatively few parameters and data input requirements. While one of our objectives is to provide a framework that can be efficiently scaled up to much larger watersheds and times scales of interest to land managers and policymakers, it is important to examine a few of the simplifying assumptions we made to conduct this study. The following five points are a brief summary of watershed characteristics relevant to biogeochemical processes and nutrient export that are not addressed in this study.

1) *Multiple species*: Aboveground and belowground biomass as well as the different species that usually populate a forested watershed is simplified by using an aggregated biomass pool. However, co-existing grass, shrubs and trees compete for nutrients, moisture and energy (i.e. interspecific competition) [*Rozzell,* 2003; *West and Chilcote,* 1968]. As a result, species tend to be spatially distributed based on their tolerance to local conditions (soil water content, nutrient availability, energy, amongst others) [*Van Breemen et al.*, 1997]. *Gholz et al.,* [1985]

found that, a few years after clearcut, the riparian zone in WS10 had the greatest annual increase in biomass and was dominated by *Aralia californica*, whereas *Senecio sylvaticus* dominated the midlands. This spatial variability in biomass accumulation and species affects biogeochemical process such as nutrient uptakes and nutrient fixation, leads to higher nutrient uptakes in the lowlands, which in turn reduces nutrient losses to the stream. Incorporating multiple species and their interactions in VELMA would reduce the amount of simulated nitrogen that reaches the stream and would allow exploration of post-harvest successional changes in the spatial and temporal distribution of species within watersheds.

2) *In stream processes*: Our simulations assume that the stream nutrient concentration reflects forest processes and do not include in-stream processes. In-stream processes are responsible for temporary retention and recycling of nutrients by a wide variety of physical, chemical and biological mechanisms [*Bilby and Likens*, 1980; *Triska et al.*, 1984; *Wallace and Benke*, 1984] such as adsorption mechanisms, algae uptake, benthic release, denitrification, and decomposition, among others [*Bernot and Dodds*, 2005], and are usually important for large watersheds and short time scales [*Tague and Band*, 2004]. *Peterson et al.,* [2001] found that in-stream processes such as nitrification rates in a third–order stream in the H.J. Andrews Experimental forest is responsible for the removal of 40% of the ammonium losses that reach the stream. Although the incorporation of in-stream processes in VELMA is beyond the scope of this paper, doing so would provide a more accurate representation of mechanisms controlling catchment-scale N export. In its present configuration, VELMA is calibrated to provide a best fit for observed N export at a particular stream sampling point, typically a stream gauging station. Thus, in-stream processes affecting measured concentrations of dissolved N are implicitly

included in this model calibration. Consequently, an explicit treatment of in-stream processes would require recalibration of the terrestrial processes controlling N transport to the stream.

3) *N fixation*: VELMA does not include the effect of N fixation on plant biomass dynamics and N cycling. N fixation can be an important source of N input into Pacific Northwest coniferous forests [*Sollins et al.*, 1980], and usually occurs during early successional stages following disturbance, when N fixing plants and microorganisms tend to be more abundant [*Rastetter et al.*, 2001]. However, this simplification is acceptable for WS10 given the low abundance of N fixers in the young, post-harvest forest. *Gholz et al.*, [1985] found that post clearcut N fixers such as red alder (*Alnus rubra*) and snowbush (*Ceanothus veluntinus*) were sparse and limited to the riparian zone of WS10.

4) *Controls on dissolved organic matter*: VELMA does not explicitly model processes that control the retention and loss of dissolved organic matter. In a field study conducted in H.J. Andrews Experimental forest, *Yano et al* [2004, 2005] found that the net production and removal of soil dissolved organic matter is controlled by the relative magnitude of hydrophobic and hydrophilic acid fractions as well as by the litter quality. For example, *Yano et al* [2005] found that root litters produced ten times more DON than other litter types (i.e. needle and wood). Other studies have shown that anions such as sulfate and phosphate compete with DOC for adsorption sites within the soil matrix, affecting retention of DOC in forest soils [*Vance and David, 1992*]. Although the incorporation of the chemical processes discussed above in VELMA is beyond the scope of this paper, doing so would provide a more accurate representation of mechanisms controlling catchment-scale DON and DOC production and export. In its present configuration, VELMA is calibrated to provide a best fit for observed DON and DOC exports. Thus, the chemical processes affecting measured concentrations of DON and DOC are implicitly

included in this model calibration. Consequently, an explicit treatment of the chemical processes would require recalibration of the terrestrial processes controlling DON and DOC transport to the stream.

5) *Soil spatial heterogeneity:* Soil texture and depth vary spatially within WS10 [*McGuire et al.*, 2007; *Ranken*, 1974; *Sayama and McDonnell*, 2009]. However, deriving high-resolution and catchment wide soil texture and depth maps from, typically, a small number of point measurements, is at best, uncertain. Instead, we assume uniform loam soil texture and uniform depth to bedrock of 2m to reflect, more or less, average conditions in the catchment [*Ranken*, 1974]. While a sensitivity analysis on the impact of the spatial distribution of soil texture and soil depth on streamflow dynamics would certainly provide insights into catchment dynamics, it is beyond the scope of this paper.

For some applications, the explicit treatment of these processes may be needed. However, it must be recognized that such added processes come at the cost of increased model complexity, computational efficiency, and applicability to larger spatial and temporal scales. These are important tradeoffs to consider, given that data needed to implement complex models are not generally available.

Appendix A: Model Description

VELMA is a spatially distributed ecohydrology model that accounts for hydrological and biogeochemical processes within watersheds. The model simulates daily to century-scale changes in soil water storage, surface and subsurface runoff, vertical drainage, carbon and nitrogen cycling in plants and soils, as well as transport of nutrients from the terrestrial landscape to the streams. VELMA consists of multi-layered soil column models that communicate with each other through the downslope lateral transport of water and nutrients (Figure A.1). Each soil column model consists of three coupled sub-models: a hydrological model, a soil temperature model, and a plant-soil model. Described below are the soil temperature and plant-soil component of the model. The hydrological component was described in a previous manuscript [*Abdelnour et al.,* 2011]. First, we describe the soil column model and then place this soil column within a catchment framework.

A.1. Soil Column Framework

We employ a multi-layer soil column as a fundamental hydrologic and ecological unit. The soil column consists of *n* soil layers (Figure A.2 and A.3). Soil water balance, soil subsurface temperature and soil C and N pools are computed for each layer.

A.1.1 The Soil Temperature Model:

The soil temperature model first simulates the ground surface temperature (*GST*) from the available mean surface air temperature (T_a) in the presence of snow cover.
The ground surface temperature is calculated as follows:

$$GST(t) = T_a \times e^{\left(\frac{SD(t)}{\lambda_{snow}}\right)} \quad (1)$$

where *SD(t)* is the snow depth (*mm*) at time *t* and λ_{snow} is the seasonal damping depth for snow which is approximately equal to 670 mm [*Hillel*, 1998] for a snowpack of density 300kgm^{-3}. In

this model, snow is an insulative material that only attenuates the mean surface air temperature signal [*Cheng et al.*, 2010]. The attenuation of the T_a signal is assumed proportional to the depth of the snowpack [*Cheng et al.*, 2010]. As a result, during snow free periods, the ground surface temperature is assumed equal to the mean surface air temperature: $SD = 0$, $GST = T_a$.

Subsurface heat transfer is then simulated using the analytical solution of the one-dimensional heat conduction equation [*Carslaw and Jaeger*, 1959; *Hillel*, 1998].
The subsurface soil temperature in layer *i* is calculated as follows:

$$T_{s,i}(d_i, t) = \overline{GST} + \left(GST\left(t - \phi(d_i, t)\right) - \overline{GST}\right) \times e^{\left(-\frac{d_i}{\lambda(t)}\right)} \quad i = 1,2 \ldots n \tag{2}$$

where $\overline{GST}$ is the annual mean soil temperature (°C), d_i is the soil depth to the middle of layer *i* (mm), $\phi(d_i, t)$ is the phase lag of $T_{s,i}$ relative to *GST* at depth d_i:

$$\phi(d_i, t) = \left(\frac{d_i}{\lambda(t)} \times \frac{360}{(2\times\pi)}\right) \quad i = 1,2, \ldots n \tag{3}$$

and $\lambda(t)$ is the damping depth of the soil (mm), defined as the characteristic depth at which the temperature signal is attenuated to *1/e* of the *GST*. $\lambda(t)$ is function of the thermal properties of the soil and the frequency of the temperature fluctuation:

$$\lambda(t) = \left(\frac{2D_h(t)}{w}\right)^{\frac{1}{2}} \tag{4}$$

where $D_h(t)$ is the time dependent thermal diffusivity of the soil (mm^2/day) and is function of the simulated soil moisture $\left(\frac{s_i}{s_i^{max}}\right)$ [*De Vries*, 1975]. For each layer *i* of the soil column:

$$\begin{aligned} D_h(t) &= \left(19.45\times10^{-3}\right)\times\left(\frac{S_i}{S_i^{\max}}\right)+2\times10^{-3} \quad && for\left(\frac{S_i}{S_i^{\max}}\right)<0.18 \\ D_h(t) &= \left(-4.055\times10^{-3}\right)\times\left(\frac{S_i}{S_i^{\max}}\right)+6.23\times10^{-3} \quad && for\left(\frac{S_i}{S_i^{\max}}\right)\geq0.18 \end{aligned} \qquad i = 1,2, \ldots n \tag{5}$$

and w is the frequency of annual temperature fluctuation (day^{-1}):

$$w = \frac{2\pi}{365} \tag{6}$$

A.1.2 The Plant-Soil Model:

The plant-soil model simulates ecosystem carbon storage and the cycling of carbon and nitrogen between a plant biomass layer and the active soil pools (Figure A.3). Specifically, the model simulates the interaction between plant biomass (*B*), soil organic carbon including humus and detritus (*SOC*), plant available soil nitrogen (*N*) including dissolved organic and inorganic nitrogen (*DON* & *DIN*) as well as dissolved organic carbon (*DOC*). The dissolved organic nitrogen (*DIN*) pool is divided into an ammonium (NH_4) and nitrate (NO_3) pool. *B*, *SOC*, NH_4, NO_3, *DON* and *DOC* pools are updated at each time step. For an *n*-layer soil model (*i=1,2…n*):

$$\frac{dB}{dt} = \left[\left(\sum_{i=1}^{n} \frac{r_i \times \mu_i \times \delta_{NH_4} \times NH_{4,i}}{NH_{4,i} \times kn}\right)\left(\sum_{i=1}^{n} \frac{r_i \times \mu_i \times \delta_{NO_3} \times NO_{3,i}}{NH_{3,i} \times kn}\right)\right] \times WS\left(\frac{s_i}{s_i^{max}}\right) \times B - m \quad (7)$$

$$\frac{dSOC_i}{dt} = r_i \times m(B) \times B - \nu_i(T_{s,i}, s_i) \times SOC_i \quad (8)$$

$$\frac{dNH_{4,i}}{dt} = n_{in} - r_i \times \mu_i \times \delta_{NH_4} \times f_M(NH_{4,i}) \times WS\left(\frac{s_i}{s_i^{max}}\right) \times B + (1-q) \times SOC_i \times \nu_i(T_{s,i}, s_i) -$$

$$Nit_i - \zeta_v(NH_{4,i}) + \zeta_v(NH_{4,i-1}) + \zeta_{l_{in}}(NH_{4,i}) - \zeta_{l_{out}}(NH_{4,i}) \quad (9)$$

$$\frac{dNO_{3,i}}{dt} = Nit_i - r_i \times \mu_i \times \delta_{NO_3} \times f_M(NO_{3,i}) \times WS\left(\frac{s_i}{s_i^{max}}\right) \times B - Den_i - \zeta_v(NO_{3,i}) +$$

$$\zeta_v(NO_{3,i-1}) + \zeta_{l\_in}(NO_{3,i}) - \zeta_{l\_out}(NO_{3,i}) \quad (10)$$

$$\frac{dDOC_i}{dt} = \alpha_{CN} \times c_d \times SOC_i \times \nu_i(T_{s,i}, s_i) - \zeta_v(DOC_i) + \zeta_v(DOC_{i-1}) + \zeta_{l\_in}(DOC_i) -$$

$$\zeta_{l\_out}(DOC_i) \quad (11)$$

$$\frac{dDON_i}{dt} = q \times SOC_i \times \nu_i(T_{s,i}, s_i) - \zeta_v(DON_i) + \zeta_v(DON_{i-1}) + \zeta_{l_{in}}(DON_i) - \zeta_{l_{out}}(DON_i) \quad (12)$$

where *m(B)* is the plant mortality rate (day^{-1}); r_i and μ_i are the biomass root fraction and the uptake rate function (day^{-1}) in layer i, respectively; δ_{NH_4} and δ_{NO_3} are the fraction of nitrogen

uptake from the ammonium and nitrate pool, respectively; SOC_i, $NH_{4,i}$, $NO_{3,i}$, DOC_i and DON_i are the soil organic carbon, ammonium, nitrate, dissolved organic carbon and dissolved organic nitrogen pools in layer *i*, respectively (gNm^{-2}); *kn* (gNm^{-2}) is the Michealis Menton calibration parameter; $WS(s_i/s_i^{max})$ is the water stress function; $v_i(T_{s,i}, s_i)$ is a first order soil organic carbon decomposition rate (day^{-1}); n_{in} is the atmospheric input of wet and dry nitrogen deposition ($gNm^{-2}day^{-1}$); $(1-q) \times SOC_i \times v_i(T_{s,i}, s_i)$ is the flux of carbon into the ammonium pool due to soil organic carbon decomposition in layer *i* ($gNm^{-2}day^{-1}$); $q \times SOC_i \times v_i(T_{s,i}, s_i)$ is the flux of carbon into the DON pool due to soil organic carbon decomposition in layer *i* ($gNm^{-2}day^{-1}$); $\alpha \times c_d \times SOC_i \times v_i(T_{s,i}, s_i)$ is the flux of carbon from the SOC pool into the DOC pool within layer *i* ($gCm^{-2}day^{-1}$); $f_M(NH_{4,i})$ *and* $f_M(NO_{3,i})$ are the Type II Michealis Menton functions for ammonium and nitrate uptake in layer *i*, respectively; Nit_i and Den_i are the ammonium nitrification ($gNm^{-2}day^{-1}$) and nitrate denitrification ($gNm^{-2}day^{-1}$) amounts in layer *i*, respectively; $\zeta_v(NH_{4i})$, $\zeta_v(NO_{3i})$, $\zeta_v(DOC_i)$, and $\zeta_v(DON_i)$ are the NH_4 ($gNm^{-2}day^{-1}$), NO_3 ($gNm^{-2}day^{-1}$), DOC ($gCm^{-2}day^{-1}$), and DON ($gNm^{-2}day^{-1}$) losses through vertical transport of water (i.e. Drainage) from layer *i* to layer *i+1*; $\zeta_{l\_out}(NH_{4i})$, $\zeta_{l\_out}(NO_{3i})$, $\zeta_{l\_out}(DOC_i)$, and $\zeta_{l\_out}(DON_i)$ are the NH_4 ($gNm^{-2}day^{-1}$), NO_3 ($gNm^{-2}day^{-1}$), DOC ($gCm^{-2}day^{-1}$), and DON ($gNm^{-2}day^{-1}$) losses out of layer *i*, through lateral transport of water (i.e. subsurface runoff) from layer *i* of the soil column to layer *i* of a downslope soil column or towards the stream; $\zeta_{l\_in}(NH_{4i})$), $\zeta_{l\_in}(NO_{3i})$), $\zeta_{l\_in}(DOC_i)$), and $\zeta_{l\_in}(DON_i)$) are the NH_4, NO_3, DOC and DON fluxes into layer *i*, through lateral transport of water (i.e. subsurface runoff) from layer *i* of an upslope soil column; α is the C:N ratio for plants and soils and is currently assumed constant for the entire simulations; c_d is the fraction of carbon that is not lost to the atmosphere due to the soil heterotrophic respiration.

A.1.2.1Atmospheric Nitrogen Deposition:

Atmospheric inputs of wet and dry nitrogen deposition are assumed to affect only the first soil layer and to be temporally distributed throughout the year as a function of precipitation.

$$n_{in} = \overline{n_{in}} \times \frac{(P_r + m)}{P_{ann}} \tag{13}$$

where $\overline{n_{in}}$ is the long-term average annual wet and dry nitrogen deposition ($gNm^{-2}yr^{-1}$), P_r is rain (mm/day), m is snowmelt (mm/day), and P_{ann} is the long-term average annual precipitation (mm/yr).

A.1.2.2 Michealis Menton functions:

The Type II Michealis Menton functions are used to limit NH_4 and NO_3 uptake.

$$f_M(NH_{4i}) = \frac{NH_{4i}}{NH_{4i} + kn} \qquad i = 1, 2 \ldots n$$
$$f_M(NO_{3i}) = \frac{NO_{3i}}{NO_{3i} + kn} \tag{14}$$

A.1.2.3 Plant Mortality:

Plant mortality rate is simulated as a function of plant biomass. *Acker et al.*, [2002] found that biomass mortality increases slowly with age for young stand until it reaches the mortality of mature and old-growth stands. In VELMA, plant mortality is assumed to increase exponentially with biomass and to reach a steady state value for mature/old-growth stands.

$$m(B) = \begin{cases} \left(\frac{(m_a \times B)^{m_b} \times m_c}{B} \right) & for\ B < B_{st} \\ m_{st} & for\ B \geq B_{st} \end{cases} \tag{15}$$

where m_a, m_b, and m_c are the mortality rate parameters, m_{st} is the equilibrium mortality rate of

old-growth stands (day^{-1}), and B_{st} is the biomass value at equilibrium for an old-growth stand (gNm^{-2} or gCm^{-2}/α).

A.1.2.4 Plant Uptake:

Plant uptake rate is assumed to increase with increasing stand age (S_{age}), reach a maximum value for young stand and then decrease and reach equilibrium value for mature/old-growth stand [*Acker et al.*, 2002; *Waring and Franklin*, 1979].

$$\mu_i = \begin{cases} \mu_{\min} + 1.44 \times \left(\frac{W_{k1}}{W_{\lambda 1}}\right) \times \left(\frac{S_{age}}{W_{\lambda 1} \times S_{age}^{\max}}\right)^{W_{k1}-1} \times e^{\left(\frac{S_{age}}{W_{\lambda 1} \times S_{age}^{\max}}\right)^{W_{k1}}} & for\ S_{age} \le S_{age}^{\max} \\ \mu_{st} + \left(\frac{W_{k2}}{W_{\lambda 2}}\right) \times \left(\frac{S_{age}}{W_{\lambda 2} \times S_{age}^{\max}}\right)^{W_{k2}-1} \times e^{\left(\frac{S_{age}}{W_{\lambda 2} \times S_{age}^{\max}}\right)^{W_{k2}}} & for\ S_{age} > S_{age}^{\max} \end{cases} \quad i = 1, 2, \ldots n \qquad (16)$$

where μ_{min} is the minimum uptake rate of plant (day^{-1}), μ_{st} is the steady state/equilibrium value of plant uptake (day^{-1}), S_{age}^{max} is the stand age for which plant uptake is the highest (days), W_{k1}, $W_{\lambda 1}$, W_{k2}, and $W_{\lambda 2}$ are the Weibull distribution parameters to calibrate.

A.1.2.5 Water Stress Function:

The water stress function varies between 0 and 1, and is proportional to the soil layer water saturation. The water stress function limits plant growth (i.e. plant nutrient uptake capacity) [*Pugnaire et al.*, 1993] as soil layer wetness approaches zero or saturation.

$$WS\left(\frac{s_i}{s_i^{\max}}\right) = \begin{cases} 0.002154 \times e^{\left(15.3511 \times \left(\frac{s_i}{s_i^{\max}}\right)\right)} & for\ \left(\frac{s_i}{s_i^{\max}}\right) < WS^{\min} \\ 1 & for\ WS^{\min} \le \left(\frac{s_i}{s_i^{\max}}\right) \le WS^{\max} \\ 2.44141 \times e^{\left(-1.116 \times \left(\frac{s_i}{s_i^{\max}}\right)\right)} & for\ \left(\frac{s_i}{s_i^{\max}}\right) > WS^{\max} \end{cases} \quad i = 1, 2, \ldots n \qquad (17)$$

where WS^{min} and WS^{max} are the minimum and maximum soil layer water saturation values between which water stress function has no effect on plant nutrient uptake.

A.1.2.6 Biomass Root Fraction:

Biomass root fraction distribution with depth follows *Gale and Grigal* [1987] model of vertical root distribution:

$$r_i = 1 - \beta^{d_i} - \sum_{j=1}^{i} r_j \qquad i=1,2,...n \tag{18}$$

where β is a fitted "extinction coefficient" that depends on the vegetation type.

A.1.2.7 Vertical Transport of Nutrient:

Vertical transport of nutrients within the soil column is a function of the vertical water drainage and the size of the nutrient pool in layer *i*:

$$\zeta_v\left(NH_{4i}\right) = qf_{NH_4} \times \frac{D_i}{s_i} \times NH_{4i} \qquad i = 1,2... n \tag{19}$$

$$\zeta_v\left(NO_{3i}\right) = qf_{NO_3} \times \frac{D_i}{s_i} \times NO_{3i} \qquad i = 1,2... n \tag{20}$$

$$\zeta_v\left(DON_i\right) = qf_{DON} \times \frac{D_i}{s_i} \times DON_i \qquad i = 1,2... n \tag{21}$$

$$\zeta_v\left(DOC_i\right) = qf_{DOC} \times \frac{D_i}{s_i} \times DOC_i \qquad i = 1,2... n \tag{22}$$

where D_i (*mm/day*) is the vertical water drainage from layer *i* to layer *i*+1 (Equation 3.14 in Chapter 3); s_i (*mm*) is the amount of water in layer *i*; $qf_{NH_4}, qf_{NO_3}, qf_{DON}$, and qf_{DOC} are the maximum fractions of NH_4, NO_3, DON and DOC pool that can be lost through transport of water.

A.1.2.8 Soil Organic Carbon Decomposition

Soil organic carbon decomposition rate varies with environmental factors such as soil temperature [*Katterer et al.*, 1998; *Lloyd and Taylor*, 1994; *Rustad and Fernandez*, 1998] and soil moisture [*Davidson et al.*, 2000] and is based on the process-based Terrestrial Ecosystem Model (TEM) presented by *Raich et al.*, [1991]. Soil moisture impacts SOC decomposition rate via moisture availability in dry soil and via oxygen availability in wet soil, such as:

$$v_i\left(T_{s,i}, s_i\right) = k_c \times F_c^{temp}\left(T_{s,i}\right) \times F_c^{moisture}\left(\frac{s_i}{s_i^{\max}}\right) \qquad i = 1, 2, \ldots n \tag{23}$$

$$F_c^{temp}\left(T_{s,i}\right) = 0.00442 \times e^{\left(0.0693 \times T_{s,i}\right)} \qquad i = 1, 2, \ldots n \tag{24}$$

$$F_c^{moisture}\left(\frac{s_i}{s_i^{\max}}\right) = 0.8 \times M_{sat}^{A} + 0.2 \qquad i = 1, 2, \ldots n \tag{25}$$

$$A = \left(\frac{\left(100 \times \left(\frac{s_i}{s_i^{\max}}\right)\right)^{ma_1} - \left(\frac{s_i}{s_i^{\max}}\right)_{opt}^{ma_1}}{\left(\frac{s_i}{s_i^{\max}}\right)_{opt}^{ma_1} - 100^{ma_1}} \right)^2 \qquad i = 1, 2, \ldots n \tag{26}$$

where k_c (day^{-1}) is the potential decomposition rate determined by model calibration; $F_c^{temp}\left(T_{s,i}\right)$ relates the microbial activity rate to changes in soil temperature (Equation 1.13; [*Raich et al.*, 1991]); $F_c^{moisture}\left(s_i/s_i^{\max}\right)$ defines the impact of soil moisture on decomposition (Equation 1.14b; [*Raich et al.*, 1991]); M_{sat} is a parameter that determines the value of $F_c^{moisture}\left(s_i/s_i^{\max}\right)$ when the soil is saturated (Table A5; [*Raich et al.*, 1991]); ma_1 is a shape parameter defining the skewness of the curve (Table A5; [*Raich et al.*, 1991]); $\left(s_i/s_i^{\max}\right)_{opt}$ is the optimal soil wetness value for which carbon decomposition is maximal; $F_c^{temp}\left(T_{s,i}\right)$ and $F_c^{moisture}\left(s_i/s_i^{\max}\right)$ vary between the values of 0 and 1.

A.1.3 Nitrification Rate:

Nitrification is the biological oxidation of ammonium into nitrite and subsequently nitrate under aerobic conditions. Nitrification occurs naturally in the environment and is carried out by autotrophic bacteria. Soil nitrification rates depend on a number of environmental factors such as soil ammonium level [*Smart et al.*, 1999], soil moisture [*Davidson et al.*, 1993], soil temperature [*Malhi and McGill*, 1982] and soil pH [*DeGroot et al.*, 1994]. In VELMA, nitrification is simulated using similar equations to the generalized model of N_2 and N_2O production of *Parton et al.*, [1996; 2001]. Soil nitrification rate is assumed to (1) increase exponentially with soil temperature ($F_N^{temp}\left(T_{s,i}\right)$; Figure 2b; [*Parton et al.*, 1996]), (2) increase as soil layer water saturation reaches optimal value for bacterial decomposition and then decrease rapidly as soil layer reaches saturation ($F_N^{moisture}\left(s_i/s_i^{\max}\right)$; Figure 2a; [*Parton et al.*, 1996]), (3) decrease exponentially as soil layer acidity (pH_i) increases ($F_N^{moisture}\left(s_i/s_i^{\max}\right)$; Figure 2c, [*Parton et al.*, 1996]), and (4) be limited by the amounted of ammonium available for nitrification.
The nitrification rate in layer *i* is calculated as follows:

$$Nit_i = K_N^{\max} \times F_N^{temp}\left(T_{s,i}\right) \times F_N^{acidity}\left(pH_i\right) \times F_N^{moisture}\left(\frac{s_i}{s_i^{\max}}\right) \times f_M\left(NH_{4i}\right) \times NH_{4i} \quad i = 1,2...n \tag{27}$$

$$F_N^{temp}\left(T_{s,i}\right) = -0.06 + 0.13 \times e^{\left(0.07 \times T_{s,i}\right)} \qquad i = 1,2...n \tag{28}$$

$$F_N^{acidity}\left(pH_i\right) = 0.56 + \frac{\arctan\left(\pi \times 0.45 \times \left(-5 \times pH_i\right)\right)}{\pi} \qquad i = 1,2...n \tag{29}$$

$$F_N^{moisture}\left(\frac{s_i}{s_i^{\max}}\right) = \left(\frac{\left(\frac{s_i}{s_i^{\max}}\right) - N_b}{N_a - N_b}\right)^{\left(N_d \times \frac{N_b - N_a}{N_a + N_c}\right)} \times \left(\frac{\left(\frac{s_i}{s_i^{\max}}\right) - N_c}{N_a - N_c}\right)^{N_d} \qquad i = 1,2...n \tag{30}$$

where $K_N^{\max}$ (day^{-1}) is the maximum nitrification rate determined by model calibration; N_a, N_b, N_c and N_d are soil parameters set according to soil texture and described in *Parton et al.,* [1996].

A.1.4 Denitrification Rate:

Denitrification is the biological reduction of nitrate under anaerobic conditions. During denitrification, heterotrophic microbes contribute to the NO_3 reduction into NO_2, NO and N_2O intermediates and ultimately into molecular nitrogen N_2 lost to the atmosphere. The denitrification process is controlled by environmental factors such as soil nitrate level, soil oxygen availability and soil labile carbon availability (e^- donor) [*Weier et al.*, 1993]. In VELMA, denitrification is simulated using the denitrification sub-model of N_2 and N_2O production presented by *Parton et al.,* [1996; 2001] and *Del Grosso et al.,* [2000]. The rate of denitrification is proportional to the amount of bio-available soil organic carbon level. However, VELMA does not differentiate between labile and non-labile soil organic matter. Therefore simulated ecosystem CO_2 loss (soil heterotrophic respiration) is used as a proxy for the amount of bio-available soil organic carbon [*Del Grosso et al.*, 2000; *Parton et al.*, 1996]. The rate of denitrification increases with decreasing oxygen availability. Oxygen availability is another critical factor not simulated by VELMA but assumed as a function of soil moisture, soil gaz diffusivity and oxygen demand. Gas diffusivity is simulated as a function of soil moisture and soil properties, whereas oxygen demand is a function of the simulated soil heterotrophic respiration [*Del Grosso et al.*, 2000; *Parton et al.*, 1996]. As a result, soil denitrification rate is simulated as a function of soil saturation $F_D^{moisture}\left(s_i/s_i^{\max}\right)$ (Equation 1, [*Parton et al.*, 2001]), soil heterotrophic respiration $F_D^{carbon}\left(CO_{2,i}\right)$ (Figure 1d, [*del Grosso et al.,* 2000]), and soil available nitrate $F_D^{nitrate}\left(NO_{3i}\right)$ (Figure 1c, [*del Grosso et al.,* 2000]). Currently VELMA simulates the total denitrification or N_2+N_2O emission without the partition between N_2 and N_2O, such that:

$$Den_i = \min\left[F_D^{carbon}\left(CO_{2i}\right), F_D^{nitrate}\left(NO_{3i}\right)\right] \times F_D^{moisture}\left(\frac{s_i}{s_i^{\max}}\right) \qquad i = 1,2...n \tag{31}$$

$$F_D^{moisture}\left(\frac{s_i}{s_i^{\max}}\right)=0.5+\frac{\arctan\left(\pi\times 0.6\times\left(0.1\times\left(\frac{s_i}{s_i^{\max}}\right)\right)-\vartheta_a\right)}{\pi} \qquad i=1,2...n \tag{32}$$

$$F_D^{carbon}\left(CO_{2,i}\right)=0.1\times\left(\alpha\times c_d\times SOC_i\times v_i\left(T_{s,i},s_i\right)\right)^{1.3} \qquad i=1,2...n \tag{33}$$

$$F_D^{nitrate}\left(NO_{3i}\right)=0.005\times\left(NO_{3i}\right)^{0.57} \qquad i=1,2...n \tag{34}$$

where $F_D^{carbon}\left(CO_{2,i}\right)$ and $F_D^{nitrate}\left(NO_{3i}\right)$represent the maximum possible N gas flux from layer *i* for a given soil heterotrophic respiration rate and nitrate level, respectively ($gNm^{-2}day^{-1}$); ϑ_a is a shape parameter that depends on soil texture; $F_D^{moisture}\left(s_i/s_i^{\max}\right)$varies between zero and 1.

A.2. Watershed Framework

To place the above described soil column framework within a catchment framework, the catchment topography is gridded into a number of pixels, with each pixel consisting of one coupled soil column. Soil columns communicate with each other through the downslope lateral transport of water and nutrients. Surface and subsurface runoff are responsible for this lateral transport and link each soil column to the surrounding downslope soil columns. A multiple flow direction method is used where flow and nutrients from one pixel to its eight neighbors is fractionally allocated according to terrain slope [*Freeman*, 1991; *Quinn et al.*, 1991]. Moreover, nutrients transported downslope from one soil column to another can be processed through the different sub-models in that downslope soil column, or continue to flow downslope, interacting with other soil columns, or ultimately discharging water and nutrients to the stream.

A.1.5 Lateral Transport of Nutrients

Lateral transport of nutrients from layer *i* of an upslope soil column to layer *i* of a

downslope soil column or towards the stream is based on the flow routing information and on terrain slope. As with the vertical transport of nutrients, the lateral transport of nutrient is a function of the lateral runoff and the size of the nutrient pool in layer *i*. For simplicity, we assume that both surface runoff and layer 1 subsurface runoff impact the nutrient pool in layer 1 of the soil column.

$$\zeta_l\left(NH_{4i}\right) = qf_{NH_4} \times \frac{\left(Q_i + q_{surf} \times Q_s\right)}{s_i} \times NH_{4i} \qquad i = 1, 2 \ldots n \tag{35}$$

$$\zeta_l\left(NO_{3i}\right) = qf_{NO_3} \times \frac{\left(Q_i + q_{surf} \times Q_s\right)}{s_i} \times NO_{3i} \qquad i = 1, 2 \ldots n \tag{36}$$

$$\zeta_l\left(DON_i\right) = qf_{DON_i} \times \frac{\left(Q_i + q_{surf} \times Q_s\right)}{s_i} \times DON_i \qquad i = 1, 2 \ldots n \tag{37}$$

$$\zeta_l\left(DOC_i\right) = qf_{DOC_i} \times \frac{\left(Q_i + q_{surf} \times Q_s\right)}{s_i} \times DOC_i \qquad i = 1, 2 \ldots n \tag{38}$$

with $q_{surf} = \begin{cases} 1 & for\ i = 1 \\ 0 & for\ i = 2, 3 \ldots n \end{cases}$

where Q_i (mm/day) is the lateral subsurface runoff from layer *i* (Equation A16; [*Abdelnour et al.*, 2011]; Q_s (mm/day) is the surface runoff that impact the nutrients pools in layer 1 (Equation A18; [*Abdelnour et al.*, 2011]).

Appendix B:

Table B.1: Model parameter values used to simulate the biogeochemical processes of watershed 10 in the H.J. Andrews Experimental Forest.

Parameters	Definition	Value	References
λ_{snow}	Seasonal damping depth for snow (mm)	670	*Hillel,* [1998]
$\overline{GST}$	Annual mean soil temperature (*°C*)	8.5	*Sollins and McCorison,* [1981]
kn	Michealis Menton calibration parameter (gN/m^2)	0.1	Calibrated
δ_{NO3}	Fraction of nitrogen uptake from the nitrate pool	0.3	*Rygiewicz and Bledsoe,* [1986]; *Kamminga-Van Wijk and Prins.,* [1993]
δ_{NH4}	Fraction of nitrogen uptake from the ammonium pool	0.7	*Rygiewicz and Bledsoe,* [1986]; *Kamminga-Van Wijk and Prins.,* [1993]
α_{CN}	C:N ratio for plants and soils	50	*Sollins and McCorison,* [1981]
c_d	Fraction of carbon that is not lost to the atmosphere due to the soil heterotrophic respiration	0.004	Calibrated
$\overline{n_{in}}$	Annual wet and dry deposition of atmospheric N ($gNm^{-2}yr^{-1}$)	0.2	*Sollins et al*., [1980]
β	Fitted extinction coefficient	0.976	*Jackson et al*., [1996]
q	Fraction of carbon decomposition that feeds into the DON pool	0.015	Calibrated
m_{st}	Steady state average mortality rate of old-growth forest (yr^{-1})	0.0125	*Lutz and Halpern*., [2006]
B_{st}	Average biomass value for an old-growth forest (gN/m^2)	42350	*Harmon et al*., [2004]; *Sollins et al.,* [1980]
m_a	Mortality rate parameter	1.55	Fixed a priori
m_b	Mortality rate parameter	4	Fixed a priori
m_c	Mortality rate parameter	1.E-14	Fixed a priori
μ_{min}	Minimum uptake rate of vegetation after disturbance (yr^{-1})	0.20	Fixed a priori
μ_{st}	Steady state value of plant uptake (yr^{-1})	0.25	Calibrated
S_{age}^{max}	Stand age for which plant uptake is the highest (years)	35	*Luyssaert et al*., [2008]
W_{k1}	Weibull distribution parameter for plant uptake	1.60	Fixed a priori
$W_{\lambda 1}$	Weibull distribution parameter for plant uptake	1.70	Fixed a priori
W_{k2}	Weibull distribution parameter for plant uptake	0.95	Fixed a priori
$W_{\lambda 2}$	Weibull distribution parameter for plant uptake	0.85	Fixed a priori
WS^{min}	Lower limit of soil water saturation, below which plant uptake is reduced (%).	40	Fixed a priori
WS^{max}	Upper limit of soil water saturation, above which plant uptake is reduced (%).	80	Fixed a priori
k_c	Potential carbon decomposition rate (vegetation dependent) (yr^{-1})	0.45	Calibrated
M_{sat}	Parameter that determines the value $F_N^{moisture}(s_i/s_i^{max})$	0.25	*Raich et al*., [1991]
ma_1	Shape parameter defining the skewness of the $F_N^{moisture}(s_i/s_i^{max})$ curve	0.14	*Raich et al*., [1991]
	Optimal soil wetness for which decomposition is maximal	40%	*Alexander*, [1977]
pH	Average pH value for the soils in WS10	4.5	*Chaer et al*., [2009]
K_N^{max}	Maximum nitrification rate (day^{-1})	0.15	*Parton et al.,* [2001]
N_a	Soil moisture function parameter for ammonium nitrification	0.4	*Parton et al*., [1996]
N_b	Soil moisture function parameter for ammonium nitrification	1.7	*Parton et al*., [1996]
N_c	Soil moisture function parameter for ammonium nitrification	3.22	*Parton et al*., [1996]
N_d	Soil moisture function parameter for ammonium nitrification	0.007	*Parton et al*., [1996]
ϑ_a	Soil moisture function shape parameter	5.0	*Del Grosso et al*., [2000]
qf_{NH_4}	Maximum fraction of NH_4 pool that can be lost through transport of water	0.12	Calibrated
qf_{NO_3}	Maximum fraction of NH_4 pool that can be lost through transport of water	0.04	Calibrated
qf_{DON}	Maximum fraction of NH_4 pool that can be lost through transport of water	0.02	Calibrated
qf_{DOC}	Maximum fraction of NH_4 pool that can be lost through transport of water	0.06	Calibrated

Acknowledgements

The information in this document has been funded in part by the US Environmental Protection Agency. It has been subjected to the Agency's peer and administrative review, and it has been approved for publication as an EPA document. Mention of trade names or commercial products does not constitute endorsement or recommendation for use. This research was additionally supported in part by the following NSF Grants 0439620, 0436118, and 0922100. We thank Sherri Johnson, Barbara Bond, Suzanne Remillard, Theresa Valentine and Don Henshaw for invaluable assistance in accessing and interpreting various H.J. Andrews LTER data sets used in this study. Sherri Johnson also provided helpful comments on an earlier draft. Data for streamflow, stream chemistry and climate were provided by the H.J. Andrews Experimental Forest research program, funded by the National Science Foundation's Long-Term Ecological Research Program (DEB 08-23380), US Forest Service Pacific Northwest Research Station, and Oregon State University.

References:

Abdelnour, A., M. Stieglitz, F. Pan, and R. McKane (2011), Catchment Hydrological Responses to Forest Harvest Amount and Spatial Pattern, *Water Resour. Res., doi:10.1029/2010WR010165, in press.*

Alexander, M. (1977). Introduction to soil microbiology, 2nd ed. Wiley, New York.

Acker, S., C. Halpern, M. Harmon, and C. Dyrness (2002), Trends in bole biomass accumulation, net primary production and tree mortality in Pseudotsuga menziesii forests of contrasting age, *Tree Physiology*, *22*(2-3), 213.

Agee, J. (1994), Fire and weather disturbances in terrestrial ecosystems of the eastern Cascades. US Forest Service, *Pacific Northwest Research Station. General Technical Report PNW-GTR-320*.

Agee, J. K. (1990), The historical role of fire in Pacific Northwest forests, *Walstad, JD, and SR Radosevich, DV Sandberg, editors*.

Alila, Y., and J. Beckers (2001), Using numerical modelling to address hydrologic forest management issues in British Columbia, *Hydrological Processes*, *15*(18), 3371-3387.

Amaranthus, M., H. Jubas, and D. Arthur (1989), Stream Shading, Summer Streamflow and Maximum Water Temperature Following Intense Wildfire In Headwater Streams1, *on Fire and Watershed Management*, 75.

Benke, A. C. 1984. `Secondary production of aquatic insects', in Resh, V. H. and Roserber, D. M. (Eds), The Ecology of Aquatic Insects. Praeger, New York. pp. 289-322.

Bernot, M., and W. Dodds (2005), Nitrogen retention, removal, and saturation in lotic ecosystems, *Ecosystems*, *8*(4), 442-453.

Beschta, R., M. Pyles, A. Skaugset, and C. Surfleet (2000), Peakflow responses to forest practices in the western Cascades of Oregon, USA, *Journal of Hydrology*, *233*(1-4), 102-120.

Beschta, R. L. (1990), Effects of fire on water quantity and quality, *Natural and prescribed fire in Pacific Northwest forests, Walstad, J.D., S.R. Radosevich, and D.V. Sandberg (eds.). Corvallis, OR: Oregon State University Press*, 219-232.

Bilby, R., and G. Likens (1980), Importance of organic debris dams in the structure and function of stream ecosystems, *Ecology*, *61*(5), 1107-1113.

Binkley, D., P. Sollins, R. Bell, D. Sachs, and D. Myrold (1992), Biogeochemistry of adjacent conifer and alder-conifer stands, *Ecology*, 2022-2033.

Bormann, F., G. Likens, D. Fisher, and R. Pierce (1968), Nutrient loss accelerated by clear-cutting of a forest ecosystem, *Science*, *159*(3817), 882.

Bosch, J., and J. Hewlett (1982), A review of catchment experiments to determine the effect of vegetation changes on water yield and evapotranspiration, *Journal of Hydrology*, *55*(1-4), 3-23.

Cairns, M., and K. Lajtha (2005), Effects of succession on nitrogen export in the west-central Cascades, Oregon, *Ecosystems*, *8*(5), 583-601.

Carignan, R., P. D'Arcy, and S. Lamontagne (2000), Comparative impacts of fire and forest harvesting on water quality in Boreal Shield lakes, *Canadian Journal of Fisheries and Aquatic Sciences*, *57*(S2), 105-117.

Carslaw, H., and J. Jaeger (1959), Conduction of heat in solids, 2nd Edition, Oxford University Press, New York.

Chaeir, G., M. Fernandes, D. Myrold and P. Bottomley (2009), Comparative resistance and resilience of soil microbial communities and enzyme in adjacent native forest and agricultural soils, *Soil Microbiology*, 58(2*)*, 414-424.

Chanasyk, D., I. Whitson, E. Mapfumo, J. Burke, and E. Prepas (2003), The impacts of forest harvest and wildfire on soils and hydrology in temperate forests: A baseline to develop hypotheses for the Boreal Plain, *Journal of Environmental Engineering and Science*, *2*(S1), 51-62.

Cheng, Y., M. Stieglitz, and F. Pan (2010), A Simple Method to Evolve Daily Ground Temperatures From Surface Air Temperatures in Snow Dominated Regions, *Journal of Hydrometeorology*.

Creed, I., L. Band, N. Foster, I. Morrison, J. Nicolson, R. Semkin, and D. Jeffries (1996), Regulation of nitrate-N release from temperate forests: a test of the N flushing hypothesis, *Water Resources Research*, *32*(11), 3337-3354.

Daly, C., and W. McKee (2011), Meteorological data from benchmark stations at the Andrews Experimental Forest. Long-Term Ecological Research. Forest Science Data Bank, Corvallis, OR. [Database]. Available: http://andrewsforest.oregonstate.edu/data/abstract.cfm?dbcode=MS001 (16 July 2011).

Davidson, E., L. Verchot, J. Catt,nio, I. Ackerman, and J. Carvalho (2000), Effects of soil water content on soil respiration in forests and cattle pastures of eastern Amazonia, *Biogeochemistry*, *48*(1), 53-69.

Davidson, E., P. Matson, P. Vitousek, R. Riley, K. Dunkin, G. Garcia-Mendez, and J. Maass (1993), Processes regulating soil emissions of NO and N20 in a seasonally dry tropical forest, *Ecology*, *74*(1), 130-139.

De Vries, D. (1975), Heat transfer in soils, *Heat and mass transfer in the biosphere*, *1*, 594.

DeGroot, C., A. Vermoesen, and O. Cleemput (1994), Laboratory study of the emission of NO and N 2 O from some Belgian soils, *Environmental Monitoring and Assessment*, *31*(1), 183-189.

Del Grosso, S., W. Parton, A. Mosier, D. Ojima, A. Kulmala, and S. Phongpan (2000), General model for N2O and N2 gas emissions from soils due to dentrification, *Global Biogeochemical Cycles*, *14*(4).

Dingman, S. (1994), *Physical hydrology*, Prentice Hall Upper Saddle River, NJ.

Dyrness, C. (1973), Early stages of plant succession following logging and burning in the western Cascades of Oregon, *Ecology*, *54*(1), 57-69.

Franklin, J. F., and R. T. T. Forman (1987), Creating landscape patterns by forest cutting: ecological consequences and principles, *Landscape Ecology*, *1*(1), 5-18.

Fredriksen, R. (1975), Nitrogen, phosphorus and particulate matter budgets of five coniferous forest ecosystems in the western Cascades Range, Oregon, Doctoral thesis, 71 pp, Oregon State University, Corvallis.

Freeman, T. (1991), Calculating catchment area with divergent flow based on a regular grid, *Computers & Geosciences*, *17*(3), 413-422.

Gale, M. R., and D. F. Grigal (1987), Vertical root distributions of northern tree species in relation to successional status, *Canadian Journal of Forest Research*, *17*(8), 829-834.

Gholz, H., G. Hawk, A. Campbell, K. Cromack Jr, and A. Brown (1985), Early vegetation recovery and element cycles on a clear-cut watershed in western Oregon, *CAN. J. FOR. RES.*, *15*(2), 400-409.

Gholz, H. L., G. M. Hawk, A. Campbell, K. Cromack Jr, and A. T. Brown (1985), Early vegetation recovery and element cycles on a clear-cut watershed in western Oregon, *Canadian Journal of Forest Research*, *15*(2), 400-409.

Giesen, T. W. G. T., S. S. P. S. S. Perakis, and K. C. K. Cromack Jr (2008), Four centuries of soil carbon and nitrogen change after stand-replacing fire in a forest landscape in the western Cascade Range of Oregon, *Canadian Journal of Forest Research*, *38*(9), 2455-2464.

Grant, G., S. Lewis, F. Swanson, J. Cissel, and J. McDonnell (2008), Effects of forest practices on peak flows and consequent channel response: a state-of-science report for western Oregon and Washington, *General Technical Report. PNW-GTR-760. Portland, OR: USDA Forest Service, Pacific Northwest Research Station*, *76*.

Grant, R., T. Black, E. Humphreys, and K. Morgenstern (2007), Changes in net ecosystem productivity with forest age following clearcutting of a coastal Douglas-fir forest: testing a mathematical model with eddy covariance measurements along a forest chronosequence, *Tree Physiology*, *27*(1), 115.

Grant, R., N. Juma, J. Robertson, R. Izaurralde, and W. B. Mcgill (2001), Long-Term Changes in Soil Carbon under Different Fertilizer, Manure, and Rotation-- Testing the Mathematical Model ecosys with Data from the Breton Plots, *Soil Science Society of America Journal*, *65*(1), 205-214.

Grier, C., and R. Logan (1977), Old-growth Pseudotsuga menziesii communities of a western Oregon watershed: biomass distribution and production budgets, *Ecological Monographs*, *47*(4), 373-400.

Grier, C. C. (1975), Wildfire effects on nutrient distribution and leaching in a coniferous ecosystem, *Canadian Journal of Forest Research*, *5*(4), 599-607.

Griffiths, R., and A. Swanson (2001), Forest soil characteristics in a chronosequence of harvested Douglas-fir forests, *Canadian Journal of Forest Research*, *31*(11), 1871-1879.

Halpern, C., and T. Spies, (1995), Plant Species Diversity in Natural and Managed Forests of the Pacific Northwest, *Ecological Applications*, 5:913–934.

Harmon, M., K. Bible, M. Ryan, D. Shaw, H. Chen, J. Klopatek, and X. Li (2004), Production, respiration, and overall carbon balance in an old-growth Pseudotsuga-Tsuga forest ecosystem, *Ecosystems*, *7*(5), 498-512.

Harmon, M. E., and B. Marks (2002), Effects of silvicultural practices on carbon stores in Douglas-fir western hemlock forests in the Pacific Northwest, USA: results from a simulation model, *Canadian Journal of Forest Research*, *32*(5), 863-877.

Harmon, M. E., W. K. Ferrell, and J. F. Franklin (1990), Effects on carbon storage of conversion of old-growth forests to young forests, *Science*, *247*(4943), 699-701.

Harr, R., and F. M. McCorison (1979), Initial effects of clearcut logging on size and timing of peak flows in a small watershed in western Oregon, *Water Resources Research*, *15*(1), 90-94, doi:10.1029/WR1015i1001p00090.

Harr, R., A. Levno, and R. Mersereau (1982), Streamflow changes after logging 130-year-old Douglas fir in two small watersheds, *Water Resources Research*, *18*(3), 637-644, doi:610.1029/WR1018i1003p00637.

Helvey, J. (1980), Effects of a North Central Washington wildfire on Runoff and Sediment Production, *JAWRA Journal of the American Water Resources Association*, *16*(4), 627-634.

Hibbert, A. (1966), Forest treatment effects on water yield, in *Proceedings of a National Science Foundation advanced science seminar*, *International symposium on forest hydrology. Pergamon Press, USA*, edited by W.E. Sopper and H.W. Lull, pp. 527-543, Pergamon Press, New York,.

Hicke, J. A., G. P. Asner, E. S. Kasischke, N. H. F. French, J. T. Randerson, G. James Collatz, B. J. Stocks, C. J. Tucker, S. O. Los, and C. B. Field (2003), Postfire response of North American boreal forest net primary productivity analyzed with satellite observations, *Global Change Biology*, *9*(8), 1145-1157.

Hillel, D. (1998), *Environmental soil physics*, Academic Pr.

Ice, G. G., D. G. Neary, and P. W. Adams (2004), Effects of wildfire on soils and watershed processes, *Journal of Forestry*, *102*(6), 16-20.

Jackson, R.B., Canadell, J., Elheringer, J., Mooney, H.A., Sala, O.E., Schulze, E.D., 1996. A global analysis of root distributions for terrestrial biomes. *Oecologia* 108, 389–411.

Janisch, J., and M. Harmon (2002), Successional changes in live and dead wood carbon stores: implications for net ecosystem productivity, *Tree Physiology*, *22*(2-3), 77.

Johnson, S., and J. Rothacher (2009), Stream discharge in gaged watersheds at the Andrews Experimental Forest. Long-Term Ecological Research. Forest Science Data Bank, Corvallis, OR. [Database]. Available: http://andrewsforest.oregonstate.edu/data/abstract.cfm?dbcode=HF004 (16 July 2011).

Johnson, S., and R. Fredriksen (2010), Long-term precipitation and dry deposition chemistry concentrations and fluxes: Andrews Experimental Forest rain collector samples. Long-Term Ecological Research. Forest Science Data Bank, Corvallis, OR. [Database]. Available: http://andrewsforest.oregonstate.edu/data/abstract.cfm?dbcode=CP002 (31 August 2011). .

Johnson, S., and R. Fredriksen (2011), Long-term stream chemistry concentrations and fluxes: Small watershed proportional samples in the Andrews Experimental Forest. Long-Term Ecological Research. Forest Science Data Bank, Corvallis, OR. [Database]. Available: http://andrewsforest.oregonstate.edu/data/abstract.cfm?dbcode=CF002 (18 July 2011).

Jones, J. A. (2000), Hydrologic processes and peak discharge response to forest removal, regrowth, and roads in 10 small experimental basins, western Cascades, Oregon, *Water Resources Research*, *36*(9), 2621-2642, doi:2610.1029/2000WR900105.

Jones, J. A., and G. E. Grant (1996), Peak flow responses to clear-cutting and roads in small and large basins, western Cascades, Oregon, *Water Resources Research*, *32*(4), 959-974.

Jones, J. A., and D. A. Post (2004), Seasonal and successional streamflow response to forest cutting and regrowth in the northwest and eastern United States, *Water Resources Research*, *40*(5), W05203, doi:05210.01029/02003WR002952.

Kamminga-van Wijk, C., and H. Prins, 1993, The kinetics of NH_4^+ and NO_3^-, *Plant and Soil*, 151, 91-96.

Katterer, T., M. Reichstein, O. Andren, and A. Lomander (1998), Temperature dependence of organic matter decomposition: a critical review using literature data analyzed with different models, *Biology and Fertility of Soils*, *27*(3), 258-262.

Keane, R. E., P. Morgan, and S. W. Running (1996), Fire-BGC: A mechanistic ecological process model for simulating fire succession on coniferous forest landscapes of the northern Rocky Mountains. Forest Service research paper*Rep.*, Forest Service, Ogden, UT (United States). Intermountain Research Station.

Keane, R. E., C. C. Hardy, K. C. Ryan, and M. A. Finney (1997), Simulating effects of fire on gaseous emissions and atmospheric carbon fluxes from coniferous forest landscapes, *World Resource Review*, *9*(2), 177-205.

Keppeler, E. T., and R. R. Ziemer (1990), Logging effects on streamflow: water yield and summer low flows at Caspar Creek in northwestern California, *Water Resources Research*, *26*(7), 1669-1679.

Kirchner, J. W. (2003), A double paradox in catchment hydrology and geochemistry, *Hydrol. Processes*, 17, 871– 874.

Langford, K. (1976), Change in yield of water following a bushfire in a forest of Eucalyptus regnans, *Journal of Hydrology*, *29*(1-2), 87-114.

Law, B., P. Thornton, J. Irvine, P. Anthoni, and S. Van Tuyl (2001), Carbon storage and fluxes in ponderosa pine forests at different developmental stages, *Global Change Biology*, *7*(7), 755-777.

Lee, J., I. K. Morrison, J. D. Leblanc, M. T. Dumas, and D. A. Cameron (2002), Carbon sequestration in trees and regrowth vegetation as affected by clearcut and partial cut harvesting in a second-growth boreal mixedwood, *Forest Ecology and Management*, *169*(1-2), 83-101.

Lloyd, J., and J. Taylor (1994), On the temperature dependence of soil respiration, *Functional ecology*, *8*(3), 315-323.

Lutz, J. A., and C. B. Halpern (2006), Tree mortality during early forest development: a long-term study of rates, causes, and consequences, *Ecological Monographs*, *76*(2), 257-275.

Luyssaert, S., E. Schulze, A. Borner, A. Knohl, D. Hessenmoller, B. Law, P. Ciais, and J. Grace (2008), Old-growth forests as global carbon sinks, *Nature*, *455*(7210), 213-215.

Malhi, S., and W. McGill (1982), Nitrification in three Alberta soils: effect of temperature, moisture and substrate concentration, *Soil Biology and Biochemistry*, *14*(4), 393-399.

Martin, W. C., and H. Dennis (1989), Logging of mature Douglas-fir in western Oregon has little effect on nutrient output budgets, *Canadian Journal of Forest Research*, *19*(1), 35-43.

McGuire, K. J., M. Weiler, J.J. McDonnell, Integrating tracer experiments with modeling to assess runoff processes and water transit times, Advances in Water Resources, Volume 30, Issue 4, April 2007, Pages 824-837, ISSN 0309-1708, 10.1016/j.advwatres.2006.07.004.

McKane, R., E. Rastetter, G. Shaver, K. Nadelhoffer, A. Giblin, J. Laundre, and F. Chapin III (1997), Climatic effects on tundra carbon storage inferred from experimental data and a model, *Ecology*, *78*(4), 1170-1187.

Means, J., P. MacMillan, and K. CROMACK (1992), Biomass and nutrient content of Douglas-fir logs and other detrital pools in an old-growth forest, Oregon, U. S. A, *Canadian journal of forest research(Print)*, *22*(10), 1536-1546.

Mitchell, S. R., M. E. Harmon, and K. E. B. O'Connell (2009), Forest fuel reduction alters fire severity and long-term carbon storage in three Pacific Northwest ecosystems, *Ecological Applications*, *19*(3), 643-655.

Moore, R., and S. Wondzell (2005), Physical Hydrology in the Pacific Northwest and the Effects of Forest HarvestingñA Review, *Journal of the American Water Resources Association*, *41*, 753-784.

Neary, D., K. Ryan, and L. DeBano (2005), Fire effects on soil and water. USDA Forest Service, Rocky Mountain Research Station, General Technical Report RMRS-GTR-42.

Parton, W., A. Mosier, D. Ojima, D. Valentine, D. Schimel, K. Weier, and A. Kulmala (1996), Generalized model for N2 and N2O production from nitrification and denitrification, *Global Biogeochemical Cycles*, *10*(3).

Parton, W., E. Holland, S. Del Grosso, M. Hartman, R. Martin, A. Mosier, D. Ojima, and D. Schimel (2001), Generalized model for NO x and N2O emissions from soils, *Journal of Geophysical Research-Atmospheres*, *106*(D15).

Peng, C., H. Jiang, M. Apps and Y. Zhang (2002), Effects of harvesting on carbon and nitrogen dynamics of boreal forests in central Canada: a process model simulation, *Ecological Modelling*, 155(2-3), 177-189.

Peterson, B., W. Wollheim, P. Mulholland, J. Webster, J. Meyer, J. Tank, E. Marti, W. Bowden, H. Valett, and A. Hershey (2001), Control of nitrogen export from watersheds by headwater streams, *Science*, *292*(5514), 86.

Pugnaire, F., L. Serrano, and J. Pardos (1993), Constraints by water stress on plant growth, *Handbook of plant and crop stress*, 271ñ283.

Quinn, P., K. Beven, P. Chevallier, and O. Planchon (1991), Prediction of hillslope flow paths for distributed hydrological modelling using digital terrain models, *Hydrological Processes*, *5*(1), 59-79.

Raich, J., E. Rastetter, J. Melillo, D. Kicklighter, P. Steudler, B. Peterson, A. Grace, B. Moore Iii, and C. Vorosmarty (1991), Potential net primary productivity in South America: application of a global model, *Ecological Applications*, *1*(4), 399-429.

Raison, R., H. Keith, and P. Khanna (1990), Effects of fire on the nutrient-supplying capacity of forest soils, *Impact of Intensive Harvesting on Forest Site Productivity. Forest Research Institute Bulletin*, *159*, 39-54.

Ranken, D. W. (1974), Hydrologic properties of soil and subsoil on a steep, forested slope, Master's thesis, 117 pp, Oregon State University, Corvallis.

Rastetter, E., P. Vitousek, C. Field, G. Shaver, D. Herbert, and G. Gren (2001), Resource optimization and symbiotic nitrogen fixation, *Ecosystems*, *4*(4), 369-388.

Rothacher, J. (1965), Streamflow from small watersheds on the western slope of the Cascade Range of Oregon, *Water Resources Research*, *1*, 125-134, doi:110.1029/WR1001i1001p00125.

Rozzell, L. R. (2003), Species pairwise associations over nine years of secondary succession: assessing alternative explanations and successional mechanisms, Master's thesis. Utah State University, Logan, Utah.

Rustad, L., and I. Fernandez (1998), Soil warming: Consequences for foliar litter decay in a spruce-fir forest in Maine, USA, *Soil Science Society of America Journal*, *62*(4), 1072.

Rygiewicz, P., and C. Bledsoe, 1986, Effects of pretreatment conditions on ammonium and nitrate uptake by Douglas-fir seedlings, *Tree Physiology*, 1, 145-150.

Santantonio, D., R. Hermann, and W. Overton (1977), Root biomass studies in forest ecosystems. Pedobiologia, Bd. 17, S. 1-31. Paper 957, *Forest Research Laboratory, School of Forestry Oregon State University, Corvallis, Oregon*.

Sayama, T. and J. J. McDonnell (2009), A new time-space accounting scheme to predict stream water residence time and hydrograph source components at the watershed scale, *Water Resour. Res.*, 45, W07401, doi:10.1029/2008WR007549.

Schmidt, J., W. Seiler, and R. Conrad (1988), Emission of nitrous oxide from temperate forest soils into the atmosphere, *Journal of atmospheric chemistry*, *6*(1), 95-115.

Smart, D., J. Stark, and V. Diego (1999), Resource limitations to nitric oxide emissions from a sagebrush-steppe ecosystem, *Biogeochemistry*, *47*(1), 63-86.

Smithwick, E., M. Harmon, S. Remillard, S. Acker, and J. Franklin (2002), Potential upper bounds of carbon stores in forests of the Pacific Northwest, *Ecological Applications*, *12*(5), 1303-1317.

Sollins, P., and F. M. McCorison (1981), Nitrogen and carbon solution chemistry of an old growth coniferous forest watershed before and after cutting, *Water Resources Research*, *17*(5), 1409–1418, doi:1410.1029/WR1017i1005p01409. .

Sollins, P., K. Cromack Jr, F. Mc Corison, R. Waring, and R. Harr (1981), Changes in nitrogen cycling at an old-growth Douglas-fir site after disturbance, *Journal of Environmental Quality*, *10*(1), 37.

Sollins, P., C. Grier, F. McCorison, K. Cromack Jr, R. Fogel, and R. Fredriksen (1980), The internal element cycles of an old-growth Douglas-fir ecosystem in western Oregon, *Ecological Monographs*, *50*(3), 261-285.

Spies, T. A., J. F. Franklin, and T. B. Thomas (1988), Coarse woody debris in Douglas-fir forests of western Oregon and Washington, *Ecology*, *69*(6), 1689-1702.

Stednick, J. (1996), Monitoring the effects of timber harvest on annual water yield, *Journal of Hydrology*, *176*(1-4), 79-95.

Stednick, J. (2008), Long-term Water Quality Changes Following Timber Harvesting, *ECOLOGICAL STUDIES*, *199*, 157.

Stednick, J. D. (2008), *Hydrological and biological responses to forest practices: the Alsea watershed study*, Springer Verlag.

Stieglitz, M., J. Shaman, J. McNamara, V. Engel, J. Shanley, and G. Kling (2003), An approach to understanding hydrologic connectivity on the hillslope and the implications for nutrient transport, *Global Biogeochemical Cycles*, *17*(4), 1105.

Storck, P., L. Bowling, P. Wetherbee, and D. Lettenmaier (1998), Application of a GIS-based distributed hydrology model for prediction of forest harvest effects on peak stream flow in the Pacific Northwest, *Hydrological Processes*, *12*(6), 889-904.

Tague, C., and L. Band (2000), Simulating the impact of road construction and forest harvesting on hydrologic response, *Earth Surface Processes and Landforms*, *26*(2), 135-151.

Tague, C., and L. Band (2004), RHESSys: Regional Hydro-Ecologic Simulation System-An object-oriented approach to spatially distributed modeling of carbon, water, and nutrient cycling, *Earth Interactions*, *8*, 1-42.

Tague, C., L. Seaby, and A. Hope (2009), Modeling the eco-hydrologic response of a Mediterranean type ecosystem to the combined impacts of projected climate change and altered fire frequencies, *Climatic Change*, *93*(1), 137-155.

Thompson, J. (2006), Society's choices: land use changes, forest fragmentation, and conservation, *Notes*.

Tiedemann, A., T. Quigley, and T. Anderson (1988), Effects of timber harvest on stream chemistry and dissolved nutrient losses in northeast Oregon, *Forest Science*, *34*(2), 344-358.

Triska, F. J., J. R. Sedell, K. Cromack, S. V. Gregory, and F. M. McCorison (1984), Nitrogen budget for a small coniferous forest stream, *Ecological Monographs*, *54*(1), 119-140.

Turner, D. P., M. Guzy, M. A. Lefsky, and T. Van (2003), Effects of land use and fine scale environmental heterogeneity on net ecosystem production over a temperate coniferous forest landscape, *Tellus B*, *55*(2), 657-668.

Turner, D. P., M. Guzy, M. A. Lefsky, W. D. Ritts, S. Van Tuyl, and B. E. Law (2004), Monitoring forest carbon sequestration with remote sensing and carbon cycle modeling, *Environmental Management*, *33*(4), 457-466.

Valentine, T., and G. Lienkaemper (2005), 30 meter digital elevation model (DEM) clipped to the Andrews Experimental Forest. Long-Term Ecological Research. Forest Science Data Bank, Corvallis, OR. [Database]. Available: http://andrewsforest.oregonstate.edu/data/abstract.cfm?dbcode=GI002 (16 July 2011).

Van Breemen, N., A. C. Finzi, and C. D. Canham (1997), Canopy tree–soil interactions within temperate forests: effects of soil elemental composition and texture on species distributions, *Can. J. For. Res*, *27*(7), 1110-1116.

Vance, G. F., and M. B. David. (1992). Dissolved organic carbon and sulfate sorption by spodosol mineral horizons. *Soil Sci*. 154:136-144.

Vanderbilt, K., K. Lajtha, and F. Swanson (2003), Biogeochemistry of unpolluted forested watersheds in the Oregon Cascades: temporal patterns of precipitation and stream nitrogen fluxes, *Biogeochemistry*, *62*(1), 87-117.

Van Verseveld, W., J. McDonnell and K. Lajtha (2008), A mechanistic assessment of nutrient flushing at the catchment scale, *Journal of Hydrology*, 358, 268 – 287.

Vitousek, P., and W. Reiners (1975), Ecosystem succession and nutrient retention: a hypothesis, *BioScience*, *25*(6), 376-381.

Wallace, J., and A. Benke (1984), Quantification of wood habitat in subtropical coastal plain streams, *Canadian Journal of Fisheries and Aquatic Sciences*, *41*(11), 1643-1652.

Waring, R., and J. Franklin (1979), Evergreen coniferous forests of the Pacific Northwest, *Science*, *204*(4400), 1380-1386.

Weber, M., and M. Flannigan (1997), Canadian boreal forest ecosystem structure and function in a changing climate: impact on fire regimes, *Environmental Reviews*, *5*(3-4), 145-166.

Weier, K., J. Doran, J. Power, D. Walters, and A. USDA (1993), Denitrification and the dinitrogen/nitrous oxide ratio as affected by soil water, available carbon, and nitrate.

West, N. E., and W. W. Chilcote (1968), Senecio sylvaticus in relation to Douglas-fir clear-cut succession in the Oregon Coast Range, *Ecology*, *49*(6), 1101-1107.

Williams, M. R., and J. M. Melack (1997), Effects of prescribed burning and drought on the solute chemistry of mixed-conifer forest streams of the Sierra Nevada, California, *Biogeochemistry*, *39*(3), 225-253.

Wimberly, M. C. (2002), Spatial simulation of historical landscape patterns in coastal forests of the Pacific Northwest, *Canadian Journal of Forest Research*, *32*(8), 1316-1328.

Wright, C. S., and J. K. Agee (2004), Fire and vegetation history in the eastern Cascade Mountains, Washington, *Ecological Applications*, *14*(2), 443-459.

Wright, H. E., and M. L. Heinselman (1973), The ecological role of fire in natural conifer forests of western and northern North America: introduction. Quaternary Research 3:319 –328.

Wright, P., M. Harmon, and F. Swanson (2002), Assessing the effect of fire regime on coarse woody debris, *USDA Forest Service General Technical Report PSW-GTR*, *181*, 621-634.

Yanai, R. D., W. S. Currie, and C. L. Goodale (2003), Soil carbon dynamics after forest harvest: an ecosystem paradigm reconsidered, *Ecosystems*, *6*(3), 197-212.

Yano, Y., K. Lajtha, P. Sollins and B. Caldwell, (2004), Chemical and seasonal controls on the dynamics of dissolved organic matter in a coniferous old-growth stand in the Pacific Northwest, USA, *Biogeochemistry*, 71, 197-223.

Yano, Y., K. Lajtha, P. Sollins and B. Caldwell, (2005), Chemistry and dynamics of dissolved organic matter in a temperate coniferous forest on andic soil: effects of litter quality, *Ecosystems*, 8, 286-300.

Figure Captions:

Figure 1: The study site is the watershed 10 (WS10) of the H. J. Andrew Experimental Forest located in the western Cascade Range of Oregon. The red dots represent the locations of the stream gages. The black triangles represent the locations of the meteorological stations.

Figure 2: Schematics of the historical events that shaped the landscape in WS10: a natural stand-replacing fire that occurred in 1525 [*Wright et al*., 2002] and a 100% man-made clearcut in 1975. The three periods of interest are: a) the post-fire recovery period from 1525 to 1968, b) the old-growth period (1969-1974) chosen at the end of the post fire recovery period where temperature and precipitation data are available to drive the model, and c) the post-harvest period from 1975 to 2008.

Figure 3: Simulated biomass (red-line) and soil organic carbon (blue-line) recovery after the 1525 stand-replacing fire. The black-dots are the observed [*Janisch and Harmon*, 2002] accumulation of bole biomass (multiplied by 1.3 to get total plant biomass) for a 500-year chronosequence of 36 Pseudotsuga-Tsuga dominated forest stands in southwestern Washington State. The x-axis is years since disturbance or age of the stand.

Figure 4: Normalized absolute errors for various adjustments of soil layer thickness

Figure 5: Simulated net primary production (red-line), net ecosystem production (blue-line) and soil heterotrophic respiration (green dashed line) recovery after the 1525 stand-replacing fire. The x-axis is years since disturbance or age of the stand.

Figure 6: Comparison between the simulated post-fire 10-year moving average of ecosystem net primary production NPP (blue-line) and the observed (1) NPP of temperate forests (red dots are individual forest stands sampled throughout the world; dashed red line is a 10-year moving average) [*Luyssaert et al*., 2008], and (2) NPP of boles for Pacific Northwest coniferous forests (black dots and solid black line) as a function of stand age (i.e. time after stand-replacing disturbance) [*Acker et al*., 2002].

Figure 7: Simulated recovery of plant biomass ($kgCm^{-2}$; red-line), soil organic carbon ($kgCm^{-2}$; blue-line), net primary production ($gCm^{-2}yr^{-1}$; black-dashed line), net ecosystem production ($gCm^{-2}yr^{-1}$; black-line), and soil heterotrophic respiration ($gCm^{-2}yr^{-1}$; green-line) after a 100% clearcut in 1975. The x-axis represents the 1975-2008 period of available precipitation and temperature data.

Figure 8: Simulated (red-dots) versus observed (black-dots) nitrate NO_3 ($mgNm^{-2}$), ammonium NH_4 ($mgNm^{-2}$), DON ($mgNm^{-2}$), and DOC losses ($mgCm^{-2}$) to the stream after the 1975 clearcut of watershed 10 in the H.J. Andrews. The simulated values are averages over the same time interval as the observed values. The x-axis represents the selected set of data between 2000 and 2007 for nitrate, ammonium and DON losses and between 2002 and 2007 for DOC losses. The y-axis represents the amount of daily losses that reaches the stream.

Figure A.1: Conceptual catchment modeling framework using multi-layered soil columns

Figure A.2: The soil column hydrological framework consists of 4-layer soil column, a standing water layer, and a snow layer. *DTB* is the soil column depth to bedrock. Δz_i, Ks_i, $\phi_{i,}$, and s_i, are the thickness, the saturated hydraulic conductivity, the soil porosity, and the soil water storage of layer *i*, respectively; *P*, P_s and P_r, are the precipitation, snow, and rain, respectively; *m* is the snowmelt and s_{SWE} is the snow water equivalent depth; *I* is the infiltration and s_{STW} is the standing water amount; Q_s is the surface runoff; Q_i, D_i and ET_i, are the subsurface runoff, the drainage and the evapotranspiration of layer i, respectively.

Figure A.3: The soil column biogeochemical framework simulates ecosystem carbon storage and the cycling of carbon and nitrogen between a plant biomass layer and a 4-layer soil column. *B* is the aboveground and belowground plant biomass. DIN_i is the dissolved inorganic nitrogen pool in layer *i*. The *DIN* pool consists of a nitrate pool and an ammonium pool, and constitutes the available soil nitrogen for plant uptake. Nit_i is the ammonium nitrification into nitrate in layer *i* (Yellow Arrow). The NO_3 pool decomposes through denitrification, which releases N_2-N_2O gases into the atmosphere. n_{in} is the atmospheric wet and dry nitrogen deposition and is accounted for in the first layer nitrogen pool. DON_i and DOC_i are the dissolved organic nitrogen and carbon pool in layer *i*, respectively. SOC_i is the soil organic carbon pool in layer *i.* Plant mortality is a source of carbon into the *SOC* pool. The *SOC* pool decomposes through soil microbial activity into *DON*, *DOC*, and NH_4 (Red Arrows). Soil heterotrophic respiration R_h from *SOC* decomposition in each layer *i* is released into the atmosphere. NO_3, NH_4, *DON* and *DOC* are soluble and transported through water drainage from layer i to layer *i+1*, and through subsurface runoff from layer *i* of the soil column to layer *i* of a downslope soil column (Blue Arrows). $\zeta_{v,i}$ is the vertical losses of nutrients from layer *i* to layer *i+1*. $\zeta_{l\_in\_i}$ and $\zeta_{l\_out\_i}$ are the lateral soluble nutrients in and out of layer *i*.

Tables:

Table 1: Comparison of the post-fire simulation results, for the period 1960-1968, when the ecosystem is considered in steady state (i.e. old-growth condition) against observed old-growth values at other Pacific Northwest Forest.

Output Parameter	Simulated Mean Value	Simulated Range of Values	Observed Mean Value	Observed Range of Values	Reference
DIN Loss ($gNm^{-2}yr^{-1}$)	0.03	0.012-0.05	0.040	0.019-0.06	*Sollins et al.,* [1980]
DON Loss ($gNm^{-2}yr^{-1}$)	0.12	0.09-0.17	0.09	0.075-0.11	*Sollins and McCorison* [1981]
DOC Loss ($gCm^{-2}yr^{-1}$)	1.8	1.3-2.4	3.18	2.0-4.3	*Sollins and McCorison* [1981]
			3.000	1.0-10.0	*Grier and Logan* [1977]
Plant Biomass (gC/m^2)	42,500	42,300-42,600	39,807	34,800-44,800	*Harmon et al.,* [2004]
			45,500	14,700-60,600	*Smithwick et al.,*[2002]
			43,500	---	*Grier and Logan* [1977]
Soil Organic Carbon (gC/m^2)	25,600	25,500-25,800	22,092	20,600-23,600	*Harmon et al.,* [2004]
			19,000	---	*Grier and Logan* [1977]
			39,600	---	*Means et al.,* [1992]
			27,500	7,500-50,000	*Smithwick et al.,*[2002]
Total Carbon Storage (gC/m^2)	68,100	67,800-68,400	61,899	56,600-67,700	*Harmon et al.,* [2004]
			62,400	---	*Grier and Logan* [1977]
Heterotrophic Soil Respiration ($gCm^{-2}yr^{-1}$)	488	457-549	577	479 to 675	*Harmon et al.,* [2004]
Denitrification Rate ($gNm^{-2}yr^{-1}$)	0.05	0.04-0.06	0.04	0.03-0.09	*Schmidt et al.,* [1988]
			0.013	0.008-0.021	*Binkley et al.,* [1992]
NPP ($gCm^{-2}yr^{-1}$)	498	463-563	597	453 to 741	*Harmon et al.,* [2004]
			544	---	*Grier and Logan* [1977]
NEP ($gCm^{-2}yr^{-1}$)	9	5-10	20	(-116) to (+156)	*Harmon et al.,* [2004]
			44	---	*Grier and Logan* [1977]

Table 2: Normalized absolute errors for various adjustments of hydrological and biogeochemical parameters.

Sensitivity Analysis	Hydrological Parameters			Biogeochemical Parameters					
	Ks	fv	fl	qf_{NH4}	qf_{NO3}	qf_{DON}	qf_{DOC}	q	nin
20% Increase	1.3	1.03	1.2	1.1	1.2	1.12	1.01	1.7	1.005
10% Increase	1.05	1.02	1.04	1.0	1.03	1.01	1.0	1.5	1.0
10% decrease	NaN	NaN	NaN	1.0	1.0	1.0	1.0	1.01	1.0
20% decrease	NaN	NaN	NaN	1.1	1.0	1.03	1.0	1.2	1.003

Table 3: Comparison of simulation results from the old-growth simulation against observed values at WS10 and other old-growth Pacific Northwest Forests.

Output Parameter	Simulated Mean Value	Observed Mean Value	Reference
NH_4 Loss ($gNm^{-2}yr^{-1}$)	0.023 (0.018-0.03)	0.01	*Vanderbilt et al.*, [2003]
NO_3 Loss (gN/m^2yr)	0.008 (0.003-0.01)	0.01 (0.009-0.011)	*Martin and Harr* [1989]
		0.003	*Vanderbilt et al.*, [2003]
DIN Loss (gN/m^2yr)	0.032 (0.02-0.04)	0.04 (0.01937-0.06)	*Sollins et al.*, [1980]
DON Loss (gN/m^2yr)	0.14 (0.12-0.18)	0.089 (0.0745-0.1043)	*Sollins and McCorison* [1981]
DOC Loss (gC/m^2yr)	2.94 (1.7-4.54)	3.178 (2.015-4.34)	*Sollins and McCorison* [1981]
		3 (1-10)	*Grier and Logan* [1977]
$\frac{\text{NH}_4\text{ Loss}}{\text{NO}_3\text{ Loss}}$	3	2	*Vanderbilt et al.*, [2003]
$\frac{\text{NH}_4\text{ Loss}}{\text{Total N Loss}}$	14%	18-33%	*Sollins and McCorison* [1981]
$\frac{\text{DON Loss}}{\text{Total N Loss}}$	81%	80%	*Vanderbilt et al.*, [2003]
$\frac{\text{DOC Loss}}{\text{DON Loss}}$	21 (14-36)	21-52	*Cairns and Lajtha* [2005]
Q vs DON	R^2=0.8	R^2= (0.4-0.79)	*Vanderbilt et al.*, [2003]
Q vs NH_4	R^2=0.6	R^2= 0.51	*Vanderbilt et al.*, [2003]

Table 4: Streamflow and nutrient losses modeling skills for the post-harvest period (1975-2008) (Observed daily streamflow from 1975 to 2008; Observed tri-weekly NH_4 ($mgNm^{-2}yr^{-1}$), NO_3 ($mgNm^{-2}yr^{-1}$), and DON ($mgNm^{-2}yr^{-1}$) losses from 1979 to 2007; Observed tri-weekly DOC ($mgCm^{-2}yr^{-1}$) losses from 2001 to 2007).

Parameter	Streamflow and Nutrient Losses Modeling Skills		
	Correlation Coefficient R^2	**Baseline adjusted modified index of agreement d'_1**	**Root Mean Square Error RMSE**
Streamflow	0.91	0.82	3.34
NH_4 Loss	0.7	0.52	0.02
NO_3 Loss	0.47	0.18	0.64
DON Loss	0.82	0.5	0.06
DOC Loss	0.94	0.84	0.19

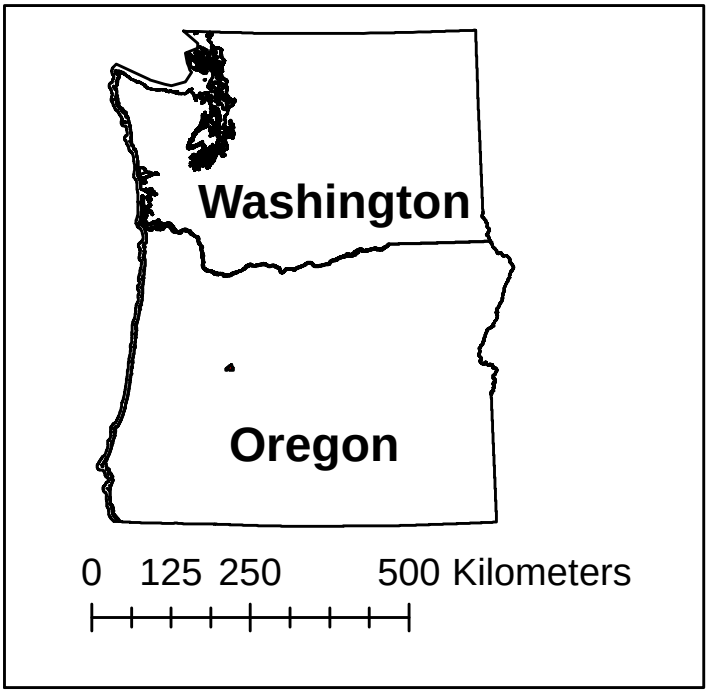

Legend

- Stream Gages
- Meteorological Stations
- Stream Network

N
W E
S

HJA DEM

Value

High : 1615

Low : 411

0 1,250 2,500 5,000 Meters

Legend

WS10 Elevation

Value

High : 700m

Low : 430m

0 125 250 500 Meters

VANMED
VANMET
8
7
6
H15MET
CENMET
GSMACK
MACK
UPLMET
10
CS2MET
PRIMET
3
2
1
9

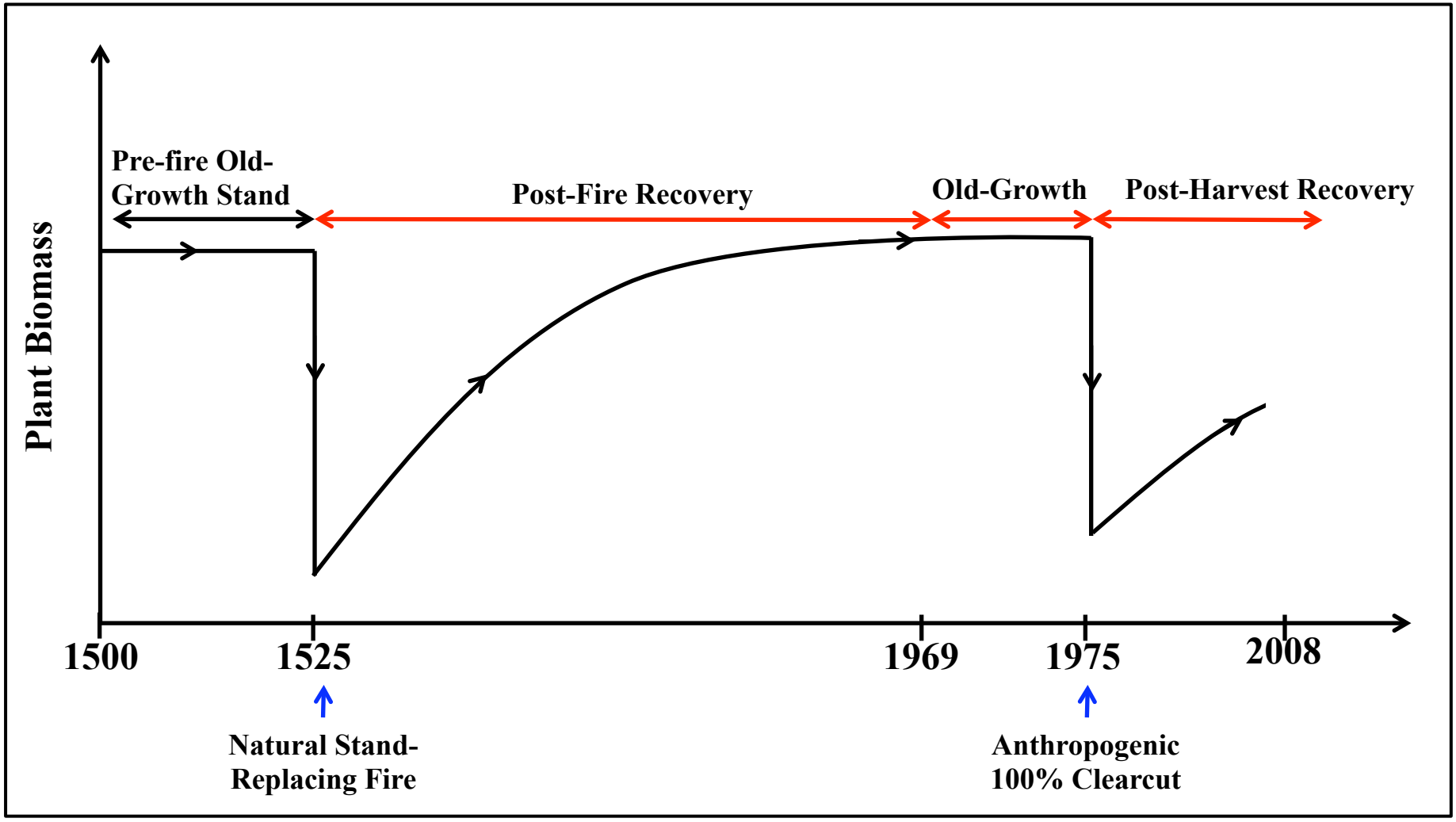
Plant Biomass
Pre-fire Old-Growth Stand
Post-Fire Recovery
Old-Growth
Post-Harvest Recovery
1500
1525
1969
1975
2008
Natural Stand-Replacing Fire
Anthropogenic 100% Clearcut


Biomass Recovery
Soil Organic Carbon Recovery
Janish and Harmon [2002]
KgC/m2
0
10
20
30
40
50
60
70
0
50
100
150
200
250
300
350
400
450
500
Years after the 1525 Fire

Equal soil layer thickness	Geometric Progression
 Δz_1=0.5m Δz_2=0.5m Δz_3=0.5m Δz_4=0.5m	 Δz_1=0.3m Δz_2=0.4m Δz_3=0.55m Δz_4=0.75m
E=1.15 >1	*E*=1.3 >1

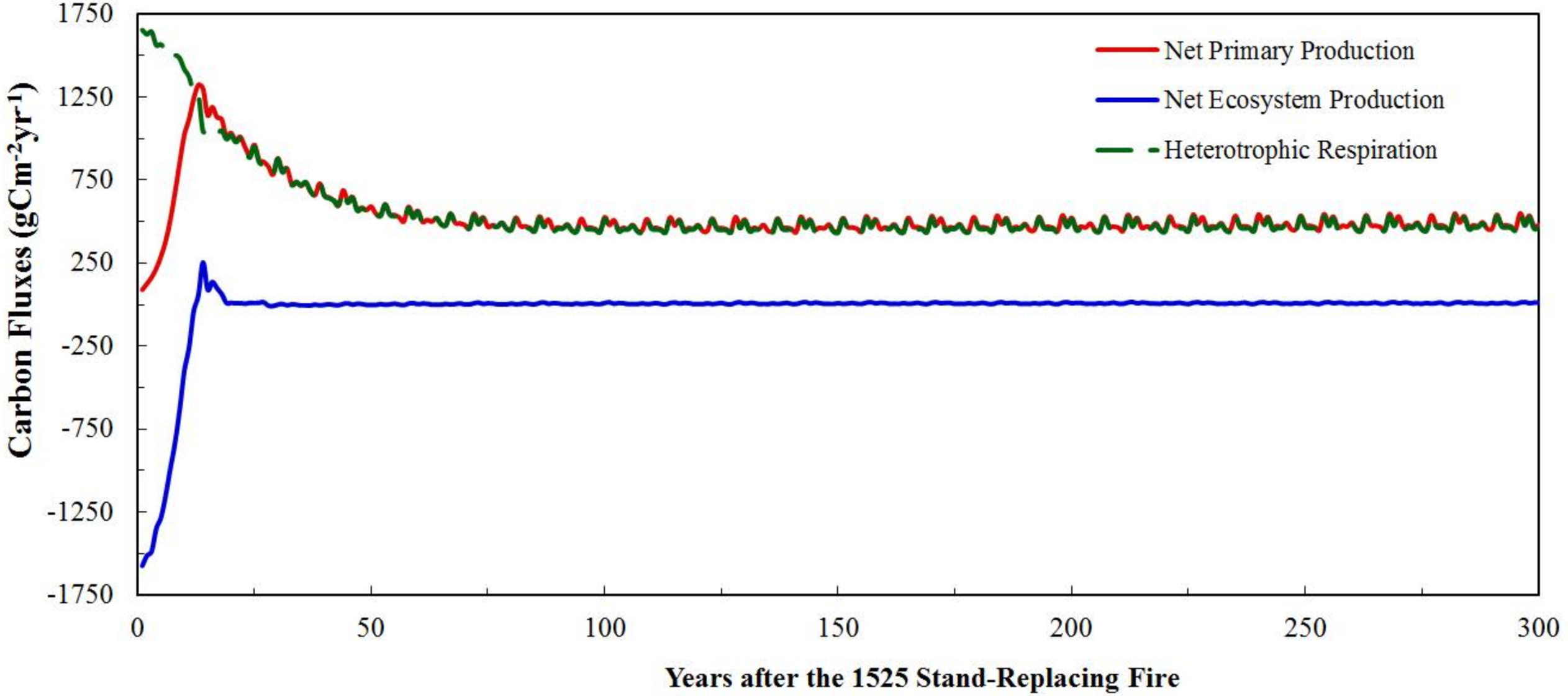
1750
1250
750
250
-250
-750
-1250
-1750
Carbon Fluxes (gCm-2yr-1)
0
50
100
150
200
250
300
Years after the 1525 Stand-Replacing Fire
Net Primary Production
Net Ecosystem Production
Heterotrophic Respiration

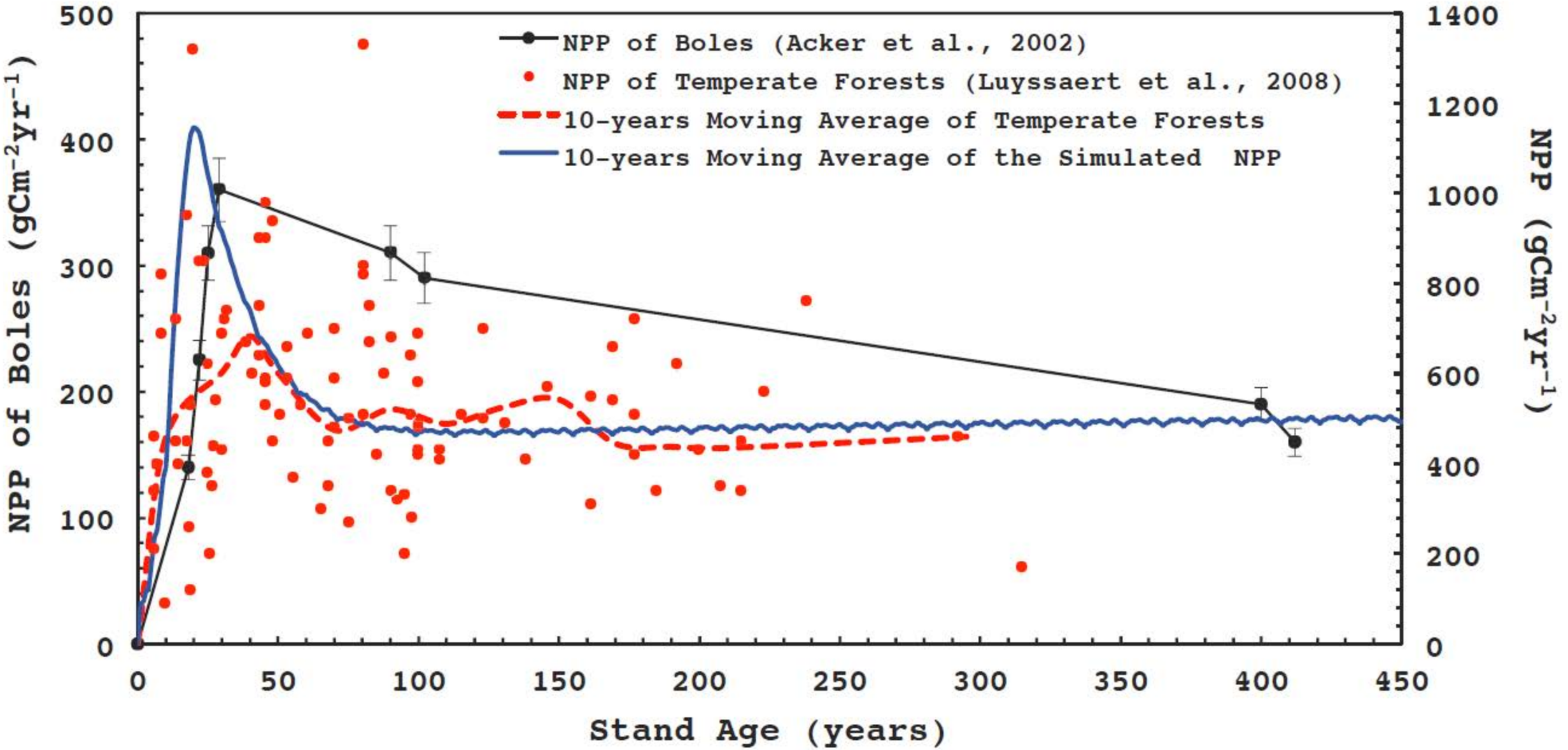
NPP of Boles (Acker et al., 2002)
NPP of Temperate Forests (Luyssaert et al., 2008)
10-years Moving Average of Temperate Forests
10-years Moving Average of the Simulated NPP
NPP of Boles (gCm-2yr-1)
NPP (gCm-2yr-1)
Stand Age (years)
0
100
200
300
400
500
0
200
400
600
800
1000
1200
1400
0
50
100
150
200
250
300
350
400
450

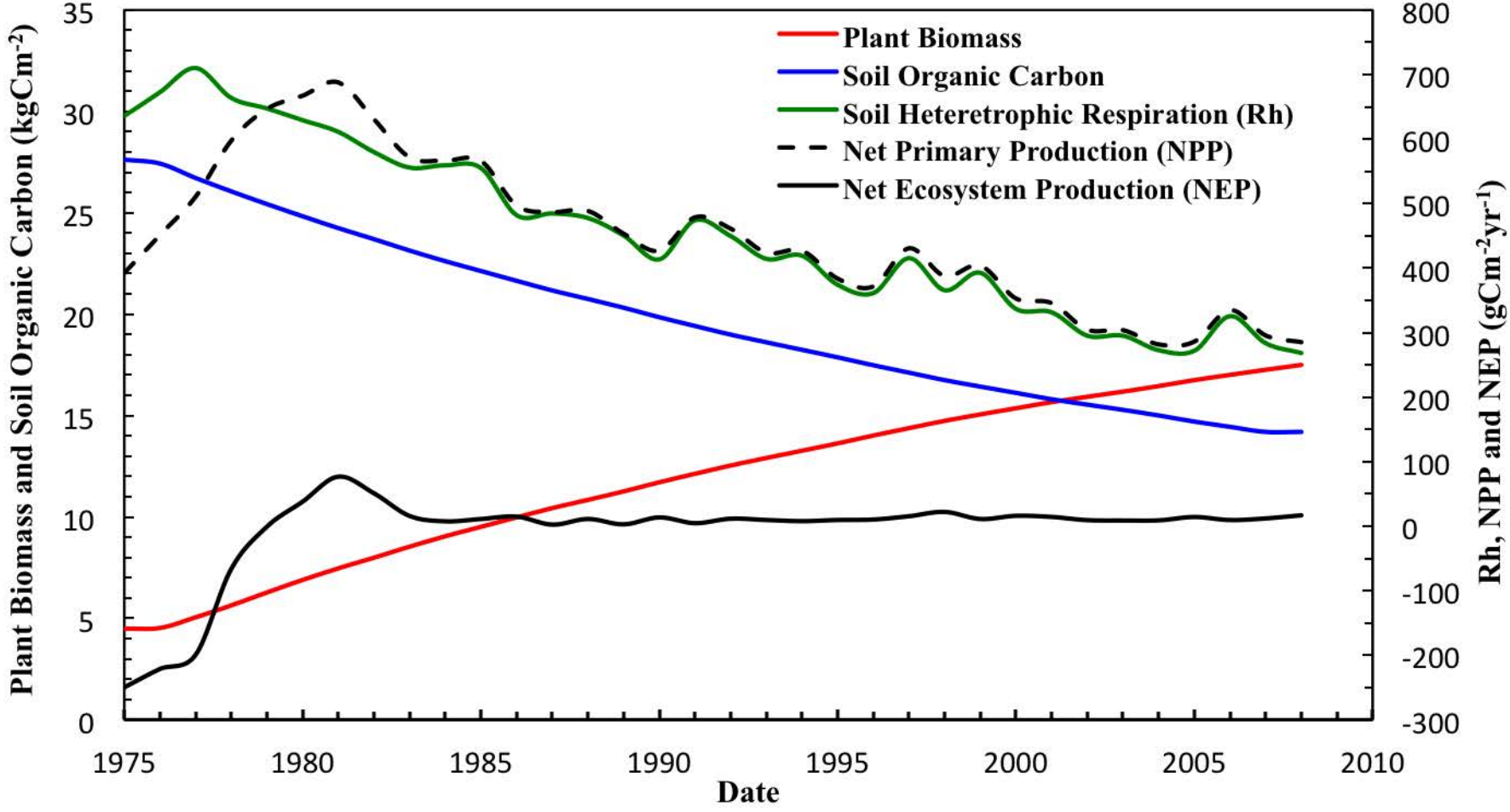
Plant Biomass
Soil Organic Carbon
Soil Heteretrophic Respiration (Rh)
Net Primary Production (NPP)
Net Ecosystem Production (NEP)
Plant Biomass and Soil Organic Carbon (kgCm-2)
Rh, NPP and NEP (gCm-2yr-1)
Date
0
5
10
15
20
25
30
35
-300
-200
-100
0
100
200
300
400
500
600
700
800
1975
1980
1985
1990
1995
2000
2005
2010

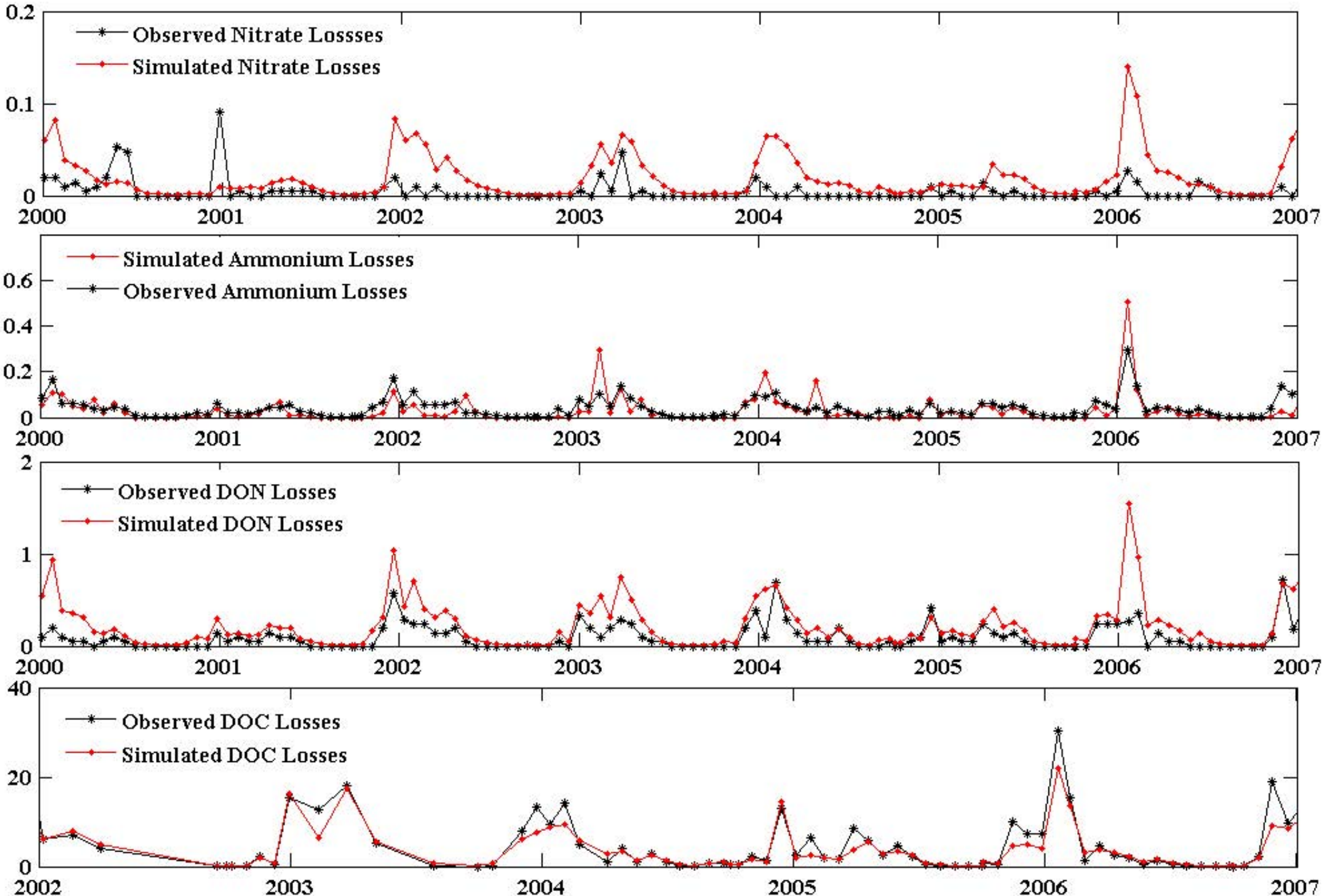
Observed Nitrate Lossses
Simulated Nitrate Losses
0.2
0.1
0
2000
2001
2002
2003
2004
2005
2006
2007
Simulated Ammonium Losses
Observed Ammonium Losses
0.6
0.4
0.2
0
2000
2001
2002
2003
2004
2005
2006
2007
Observed DON Losses
Simulated DON Losses
2
1
0
2000
2001
2002
2003
2004
2005
2006
2007
Observed DOC Losses
Simulated DOC Losses
40
20
0
2002
2003
2004
2005
2006
2007

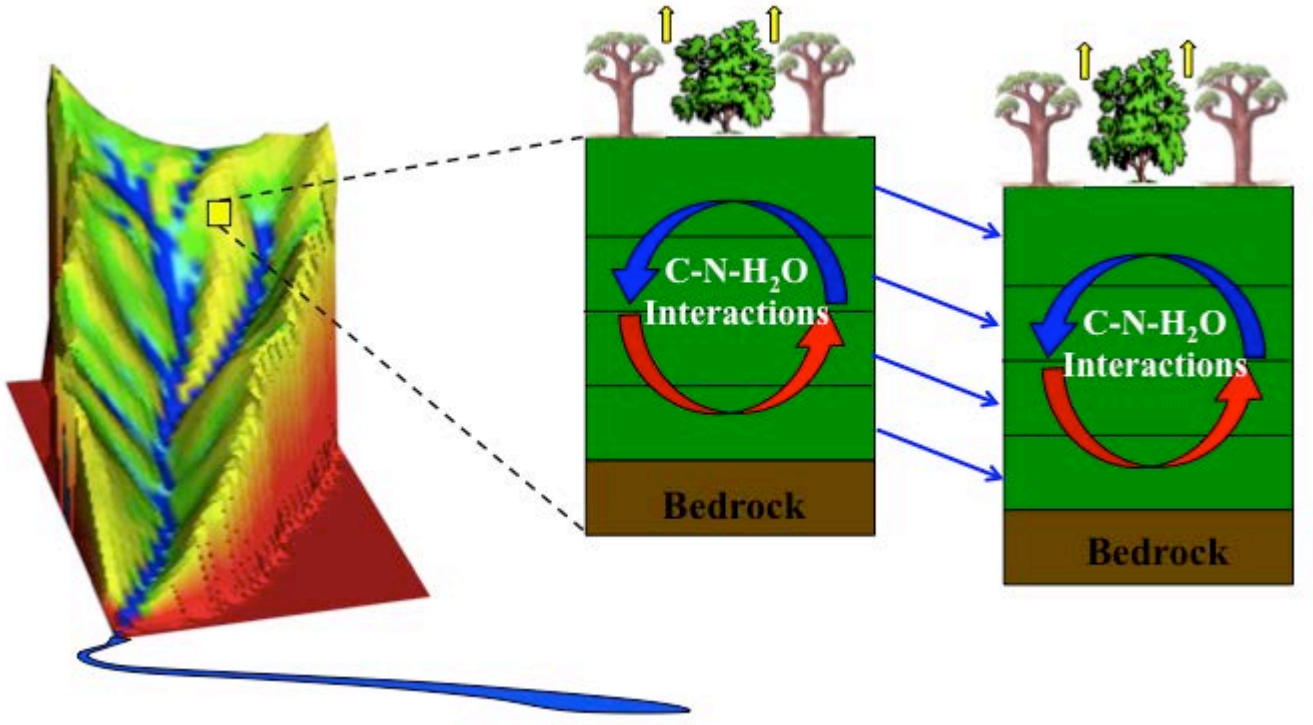
C-N-H2O
Interactions
Bedrock
C-N-H2O
Interactions
Bedrock

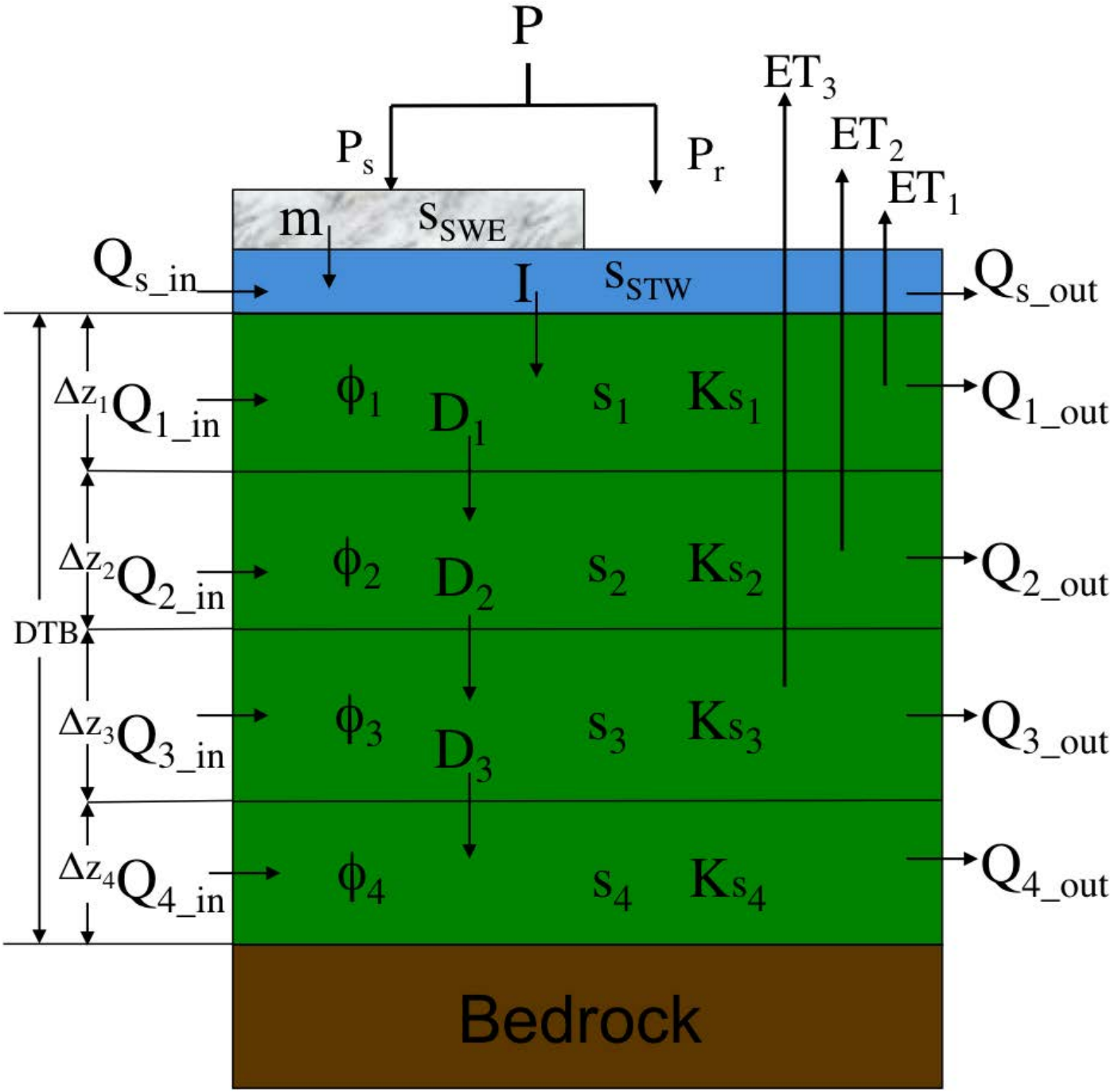
P
P_s
P_r
ET_3
ET_2
ET_1
m
s_{SWE}
Q_{s_in}
I
s_{STW}
Q_{s_out}
$\Delta z_1 Q_{1\_in}$
ϕ_1
D_1
s_1
Ks_1
Q_{1_out}
$\Delta z_2 Q_{2\_in}$
ϕ_2
D_2
s_2
Ks_2
Q_{2_out}
DTB
$\Delta z_3 Q_{3\_in}$
ϕ_3
D_3
s_3
Ks_3
Q_{3_out}
$\Delta z_4 Q_{4\_in}$
ϕ_4
s_4
Ks_4
Q_{4_out}
Bedrock

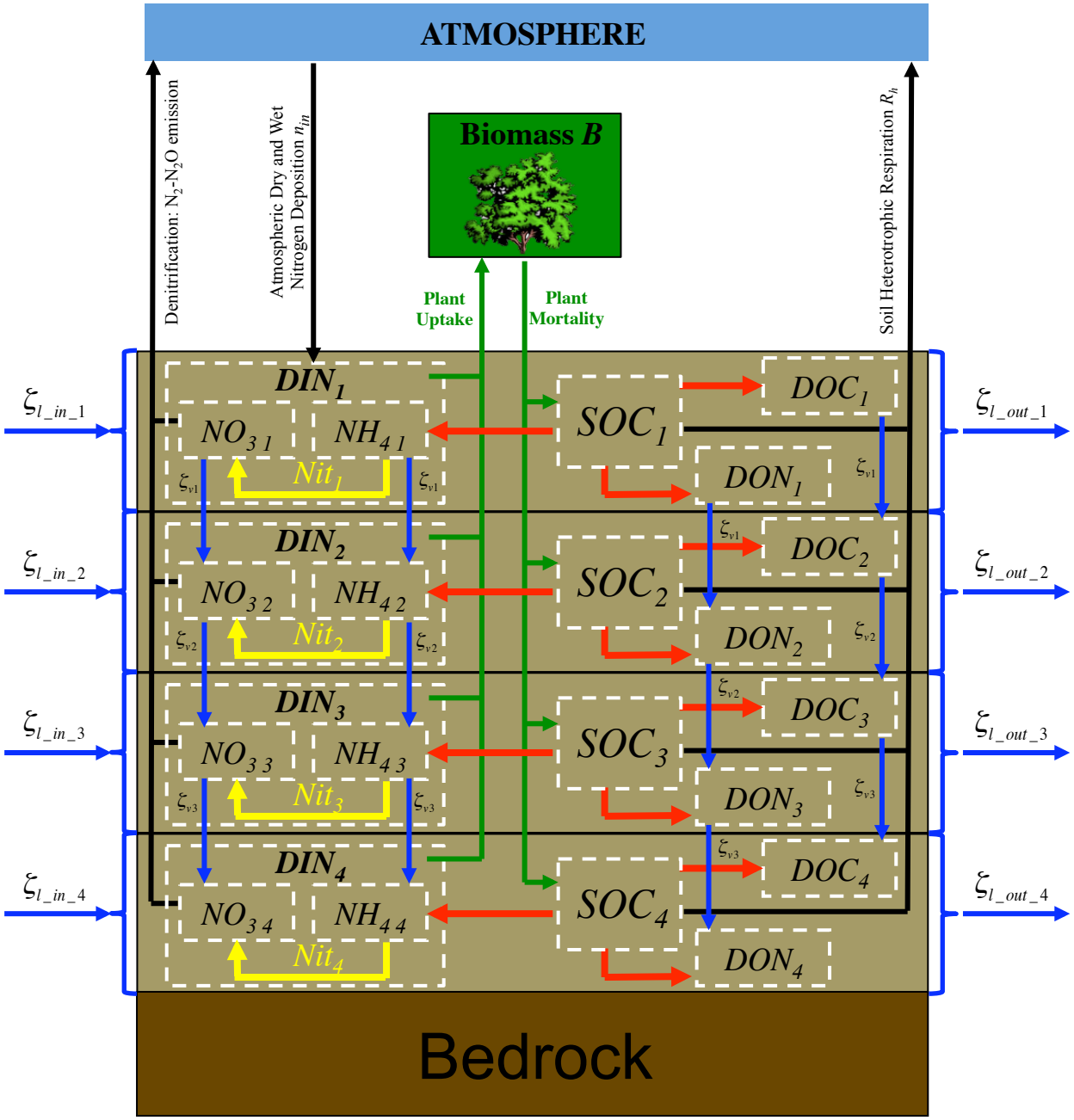
ATMOSPHERE
Denitrification: N_2-N_2O emission
Atmospheric Dry and Wet Nitrogen Deposition n_{in}
Biomass B
Plant Uptake
Plant Mortality
Soil Heterotrophic Respiration R_h
$\zeta_{l\_in\_1}$
$\zeta_{l\_in\_2}$
$\zeta_{l\_in\_3}$
$\zeta_{l\_in\_4}$
$\zeta_{l\_out\_1}$
$\zeta_{l\_out\_2}$
$\zeta_{l\_out\_3}$
$\zeta_{l\_out\_4}$
DIN_1
$NO_{3\,1}$
$NH_{4\,1}$
Nit_1
DIN_2
$NO_{3\,2}$
$NH_{4\,2}$
Nit_2
DIN_3
$NO_{3\,3}$
$NH_{4\,3}$
Nit_3
DIN_4
$NO_{3\,4}$
$NH_{4\,4}$
Nit_4
SOC_1
SOC_2
SOC_3
SOC_4
DOC_1
DOC_2
DOC_3
DOC_4
DON_1
DON_2
DON_3
DON_4
ζ_{v1}
ζ_{v2}
ζ_{v3}
Bedrock